A comprehensive approach to the mathematical modeling of mass transport in biological systems: Fundamental concepts and models

2 authors:

Shadi Zaheri
University of Texas at Dallas
7 PUBLICATIONS   **1** CITATION

SEE PROFILE

Fatemeh Hassanipour
University of Texas at Dallas
68 PUBLICATIONS   **368** CITATIONS

SEE PROFILE

Some of the authors of this publication are also working on these related projects:

Computational and Mathematical modeling for Cellular Mechanisms View project

Modeling of Reformer Chamber for Hydrogen generation system View project

Highlights

A Comprehensive Approach to the Mathematical Modeling of Mass Transport in Biological Systems: Fundamental Concepts and Models
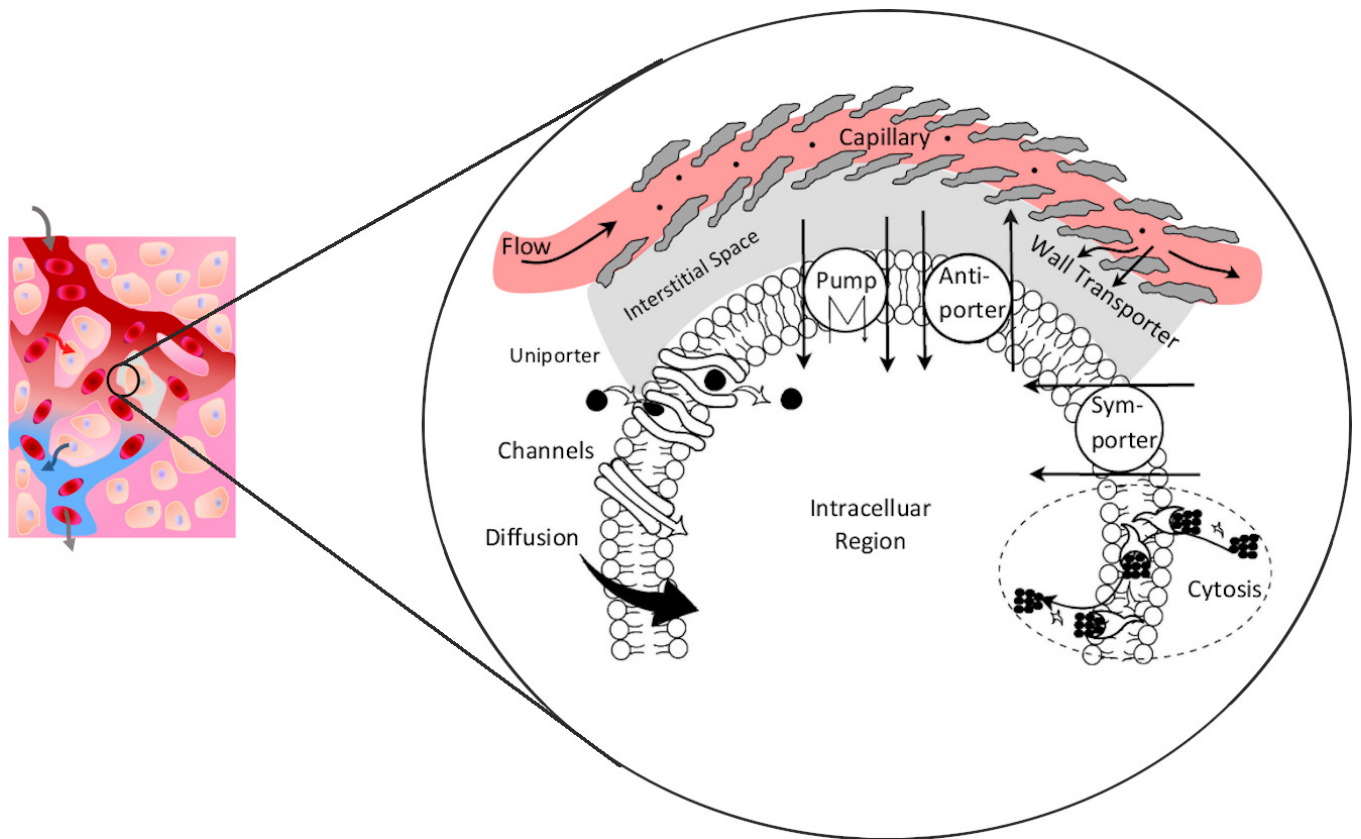
Shadi Zaheri, Fatemeh Hassanipour

- A mathematical framework for mass transport at different tissue levels is developed.
- Terminology from engineering, physiological, and biophysical viewpoints is discussed.
- The primary focus of this work is on membrane-mediated transport mechanism models.
- This work provides scientists with guidelines for biological mass transport analysis.

Graphical Abstract

A Comprehensive Approach to the Mathematical Modeling of Mass Transport in Biological Systems: Fundamental Concepts and Models

Shadi Zaheri, Fatemeh Hassanipour

A Comprehensive Approach to the Mathematical Modeling of Mass Transport in Biological Systems: Fundamental Concepts and Models [☆]

Shadi Zaheri[a], Fatemeh Hassanipour[a,*]

[a]*Department of Mechanical Engineering, The University of Texas at Dallas, Richardson, TX, 75080, USA*

Abstract

Multiscale mathematical modeling of transport phenomena across different levels of biological systems, such as cells, capillaries, tissues, and organs, has been increasingly helpful in describing how interactions among these systems lead to their function and dysfunction. The development of models across these scales is based on knowledge from various fields, such as engineering, physiology, and biophysics, and it requires significant collaboration among scientists from the relevant areas. Therefore, a unified framework to describe the fundamental principles and unite the established models could support this growing research community. In this regard, the present work deals with the essential terminology required to understand and model biological transport mechanisms, as well as to compile currently available models. An inclusive mathematical framework for models of mass transport mechanisms in different tissue compartments, including cells, capillaries, and gland ducts, is developed, with a primary focus on the mechanisms of membrane-mediated transporters such as channels, uniporters, symporters, pumps, and antiporters. The main objective of this study is to provide a comprehensive tool to facilitate the analysis of biological mass transport mechanisms and substantially decrease the time taken to find the appropriate model for a study.

Keywords: Biological Transport Mechanism, Membrane transporter, Mass Transport in Tissue's Comportment, Mathematical Modelling, Flow Transport in Biological Systems

Nomenclature

Conventions

Square brackets: Typically are used with letters (e.g., [A], [B], [EA]) to indicate the concentration of the substrate.

Subscripts E and its compounds (e.g., EA, EB, EAB): When used with reaction or transport quantities (e.g., reaction rate constants, translocation rate, concentration, flux), these refer to carrier and to the carrier-substrate complex, respectively.

Subscripts i, A, B, and C: When used with reaction or transport quantities (e.g., reaction rate constants, concentration, flux), these refer to solute $'i'$, $'A'$, $'B'$, and $'C'$, respectively.

Superscripts M and N: When used with reaction or transport quantities (e.g., concentration, flux), these refer to the transport domain in a system with multiple domains.

Physics Constants

F	Faraday's constant	$96,490$	$(A \cdot s/mol)$
K_B	Boltzmann's constant	1.38×10^{-23}	$(m^2 \cdot kg/(s^2 \cdot K))$
R	Universal gas constant	8.314	$(J/(mol \cdot K))$

Greek symbols

β_i Restriction coefficient of a solute $'i'$

Δ Operator to describe the change of any changeable quantity (e.g., $\Delta \pi^{M,N}$ is osmotic pressure difference between M and N domains)

η_h Hill coefficient

γ^M Ratio of the surface area of compartment M to tissue volume

$\hat{v}_s$ Molar volume of the solute

23	Λ_i^∞	Electrical conductance of ion $'i'$ in the solution
24	μ	Dynamic fluid viscosity
25	∇	Operator to either get the gradient tensor of a vector, the divergence of a vector or to find
26		the gradient of a scalar field
27	π	Osmotic pressure
28	$\prod$	Oncotic pressure
29	ψ	Electrical potential
30	ρ	Fluid density
31	$\sigma(y)$	Local charge density
32	σ_i	Reflection coefficient of a solute $'i'$ through the membrane
33	$\sigma_p(y)$	Charge density on the immobilized protein wall of the membrane channel
34	τ	Tortuosity coefficient
35	ε	Porosity of the wall
36	ε^M	Ratio of the volume faction occupied by compartment M to the tissue volume
37	ε_0	Dielectric constant
38	$\varnothing_w$	Solvent association factor

39 **Other Symbols**

40	$\mathbf{u}$	Fluid velocity
41	$\overline{\mathbf{u}}$	Averaged fluid velocity
42	$\overline{C_i}$	Volume-averaged molar concentration of species $'i'$

3

43 $\overline{C_i}^{M,N}$ Logarithmic mean average of the molar concentrations at the two sides of the membrane

44 $\overline{R_i}$ Volumetric reaction rate of solute $'i'$

45 $\mathbf{E}$ Electric field

46 A_p Available area of the heterogeneous porous membrane

47 a_p Radius of the membrane pores

48 A_s Surface area of the tube

49 a_s Radius of the spherical molecule/solute

50 a_t Tube radius

51 C_i Molar concentration of species $'i'$

52 C_L The concentration of unbound ligand for the Hill model

53 D_i Diffusion coefficient of species $'i'$

54 $f_o^{channel}$ Open probability of the ion channel

55 $F_{convection}$ Axial volumetric convection fluid flow rate in the tube

56 $F_{filtration}$ Volumetric filtration fluid flow rate

57 g Translocation rate constant

58 $g_{i,channel}$ Membrane conductance for channels of ion $'i'$ (channel conductance)

59 $I''_{i,channel}$ Net current density of ion $'i'$ through the ion channels

60 $J_{antiporter}$ The transported flux driven via antiporters

61 J_{ATPase} The transported flux driven via ATPase pumps

62 $J_{filtration}$ The transported flux due to the hindered convection

4

63    $J_{i,convection}$ Molar flux of solute $'i'$ by convection

64    $J_{i,diffusion}$ Molar flux of solute $'i'$ by diffusion

65    $J_{i,migration}$ Molar flux of solute $'i'$ by migration

66    $J_{i,wall}^{M}$ The net outward molar flux of solute $'i'$ from domain $'M'$ across the wall

67    $J_{ionchannel}$ The ion flux through the ion channels

68    $J_{symporter}$ The transported flux driven via symporters

69    $J_{uniporter}$ The transported flux driven via uniporters

70    $J_{waterchannel}$ The water flux through the water channels

71   K When used in the carrier-mediated transport equations (e.g., $K_A^M = k_A^{-M}/k_A^{+M}$, $K_B^M = k_B^{-M}/k_B^{+N}$),

72   it indicates the dissociation constant for a reaction step.

73   k^+ Binding rate constant (e.g., k_A^+ is the binding constant for solute A)

74   k^- Unbinding rate constant (e.g., k_A^- is the unbinding constant for solute A)

75   K_A The ligand concentration at which half-saturation is achieved, for Hill model

76   K_i^M Equilibrium constant coefficient for substrate $'i'$ in domain M

77   K_m Michaelis-Menten rate constant, which is the substrate concentration at half the maximum

78   rate (V_{max})

79   K_i^m Membrane partition coefficient for solute $'i'$

80    $L_p^{waterchannel}$ Hydraulic conductivity of the water channel

81   L_p Hydraulic conductivity (filtration coefficient) of the membrane

82   l_t Tube Length

83   M_w Molecular weight of the solvent

84 $O_i^{channel}$ The total number of open channels per unit area of the membrane

85 P Hydraulic pressure

86 P_i^m Membrane permeability coefficient to the solute $'i'$

87 T Temperature

88 t_m Membrane thickness

89 u_{wall} Transmembrane fluid flow

90 V_m Membrane voltage or membrane electric potential

91 $V_{i,rev}$ Membrane reversal potential for a single ion $'i'$

92 V_{max} Maximum reaction velocity achieved at the saturated substrate concentrations for the Michaelis-
93   Menten model

94 z_i Ionic charge number on an ion $'i'$

1. Introduction

Mass transport mechanisms in complex biological systems, such as cells, tissues, and organs, are tightly regulated; any dysregulation can result in diseases, such as membrane disorders, cancer, and other complex diseases. It is necessary to understand the relationships among transport mechanisms in different biological systems and to be able to predict their behavior under various conditions. Mathematical and computational modeling are powerful tools to describe the interactions that occur at the different levels of biological systems and to predict tissue and organ behavior under different conditions. Researchers have used mathematical models extensively to understand the diseases caused by perturbations in biological transport processes [1–9]. Interest in this area of research has grown rapidly, with many published examples demonstrating the importance of these models in the analysis of transport processes and transport-related disorders. This progress has been enabled by the coupling of experimental and computational studies at multiple scales and cooperation among researchers from different backgrounds.

Numerous mathematical models have been provided in chapters of books in the fields of biology, physiology, and engineering [10–26] as well as in research articles dealing with the neurological system [27, 28], cardiovascular system [29–32], respiratory system [33, 34], cellular level behavior [35–38], nutrient transport [39], and membrane transporters and channels [40–42], among others.

However, there is **a need to gather and examine** the work that has been done previously in order to develop an outline of the further work required to make these models more practical and improve the quality of their predictions. Furthermore, **consolidating all the models into one framework** will provide researchers with access to better alternative fitting models for different experimental/clinical analyses. In many cases, transport models that are invalid for the given operating conditions are used simply because of the lack of a better alternative model. For example, in several instances, movements of some molecules across the membrane may be assumed to happen with the constant rate, simply because of not having the relevant model describing the molecule movement through the membrane-transporters available. With collecting all the models unitedly, including those categorized based on the types of membrane transporters, there is a possibility to

7

obtain extremely more accurate model information for the mass transport mechanisms that are of interest to us. Another challenge in the area of multiscale transport modeling of biological systems is **the lack of common language** among researchers from relevant fields. This study aims to provide an interface for researchers from different fields with interest in the area of biological transport mechanisms. In this regard, the present work integrates engineering principles with relevant physiological, biophysical, and biomedical concepts and defines the essential terminology from the relevant fields. To accomplish this, a full review of mass transport models *within* and *across* individual biological systems, including capillaries, the interstitial region, cell membranes, intracellular regions of the cell, and duct lumina, has been performed. First, the essential concepts of continuity, transport, and the relevant kinetic equations and their connection to solute distribution in biological systems are outlined in sections 2 and 3. Next, a detailed discussion of the three main transport mechanisms, namely, convection, diffusion, and migration, is provided in sections 4.1, 4.2, and 4.3. An application of these models to different types of membrane-mediated transport mechanisms, including channels and carriers, along with the relevant kinetic equations, is described in sections 5.1 and 5.2. Detailed kinetic modeling approaches for membrane transporters are described without emphasizing any particular family. For each family of membrane transporters, most of the previously published models are presented and transformed into a general identical parametric form. Furthermore, our review of previously published models prompted us to derive some new kinetic models for membrane-transporter mechanisms. This work does not attempt to evaluate or analyze these models, but instead intends to provide a comprehensive modeling toolbox that should facilitate investigation of membrane transport mechanisms.

2. Model Construction

Biological systems can be categorized into different levels, ranging from cells and the interstitial region to capillaries, tissues, and organs. For a living biological system to operate, nutrients and other molecules must continuously move across the boundaries of the system at each level and participate in biochemical reactions.

In this work, a heterogeneous representative elementary volume (REV) is used to represent the tissue at a macroscopic scale (Figure 1). Next, at the microscopic scale, each of the tissue compart-

ments, including the cell, interstitial, and capillary phases, is considered as an individual control volume (CV), and the transport processes of fluids (solutions such as blood and air) and solutes (such as nutrients, hormones, electrolytes, oxygen, and carbon dioxide) across the boundaries of these control volumes is modeled.
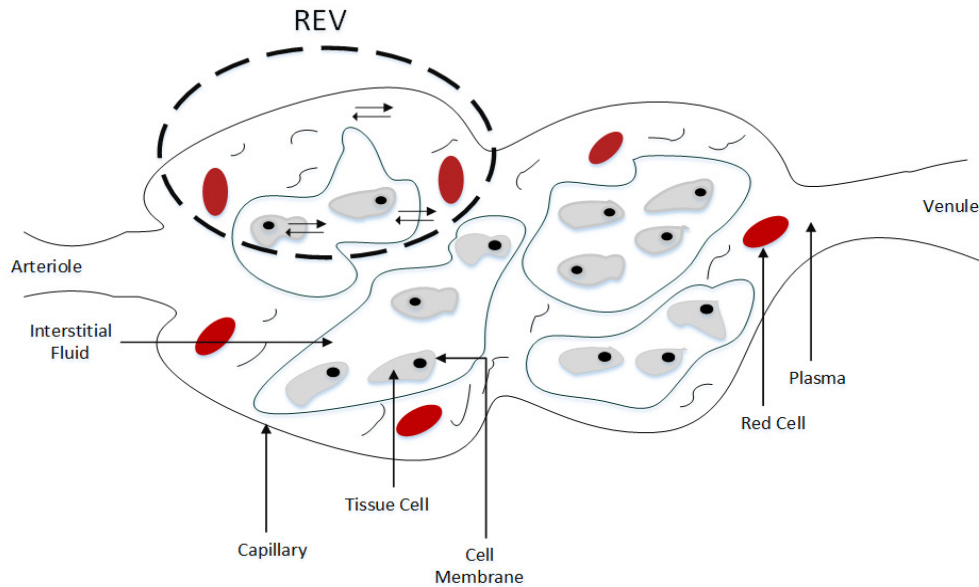

Figure 1: Representative Elementary Volume (REV) of a general tissue consists of capillary, interstitial fluid, and cells.

The models of volume-averaged fluid flow and solute transport (through the regions "M" and "N") within the defined control volumes are shown in Figure 2. For the purpose of simplification, it is assumed that the flow is incompressible, laminar, Newtonian, and that there is no fluid accumulation in the boundaries.
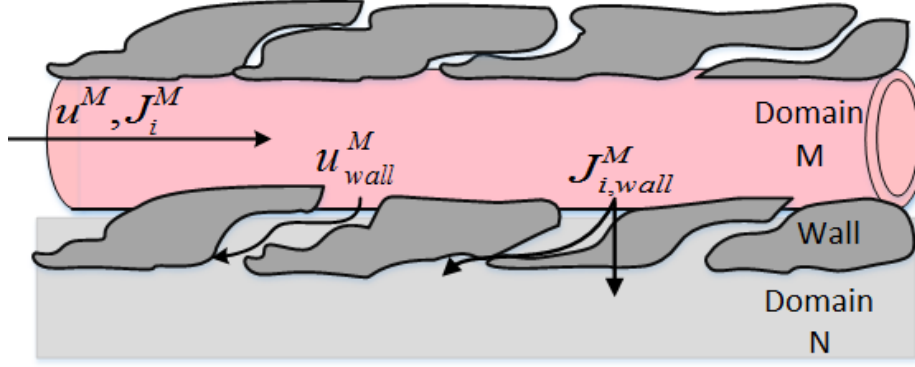
9

Figure 2: Volumetric fluid movement within a control volume (u^M) and the transmembrane flow (u_{wall}). Solute transport flux within the control volume (J_i^M) can happen by *convection*, *diffusion*, and *migration* mechanisms. $J_{i,wall}^M$ represents the net outward molar flux of solute $'i'$ from control volume $'M'$ to its adjacent compartments across the wall (e.g., N). Transport between the M and N compartments can occur either through the gaps between the cells of the wall separating the domains (the curved arrow) or across the individual cell membranes (the straight arrow).

The **macroscopic** mass and momentum continuity equations for mass transport through regions "M" and "N" are as follows [43, 44]:

$$\nabla.\bar{\mathbf{u}} = 0 \tag{1}$$

$$\frac{\partial \bar{\mathbf{u}}^M}{\partial t} + \bar{\mathbf{u}}^M.\nabla\bar{\mathbf{u}}^M = \frac{1}{\rho}\left(\mu^M \ \nabla^2\bar{\mathbf{u}}^M - \nabla\bar{P}^M\right) \tag{2}$$

Where $\mathbf{u}^M$ is the fluid velocity in region M, ρ is the fluid density, ∇P^M is the pressure drop along the tube, and μ is the dynamic fluid viscosity.

The **microscopic** form of the Navier-Stokes and mass-momentum conservation equations and the corresponding dynamic fluid flow model can be expressed using the equations below [45–48]:

$$\overline{\nabla.\mathbf{u}^M} = \nabla.\bar{\mathbf{u}}^M + \frac{\gamma^M}{\varepsilon^M}u_{wall}^M = 0 \ \Rightarrow \ \boxed{\nabla.\bar{\mathbf{u}}^M = -\frac{\gamma^M}{\varepsilon^M}u_{wall}^M} \tag{3}$$

$$\rho\left(\frac{\partial \bar{\mathbf{u}}^M}{\partial t} + \bar{\mathbf{u}}^M.\nabla\bar{\mathbf{u}}^M\right) = -\nabla\bar{P}^M + \mu^M\nabla^2\bar{\mathbf{u}}^M$$

$$\Rightarrow \ \boxed{\frac{\partial \bar{\mathbf{u}}^M}{\partial t} = -\bar{\mathbf{u}}^M.\nabla\bar{\mathbf{u}}^M + \frac{1}{\rho}\left(\mu^M \ \nabla^2\bar{\mathbf{u}}^M - \nabla\bar{P}^M\right)} \tag{4}$$

10

164 Where γ^M is the ratio of the surface area of compartment M to tissue volume and ε^M is the ratio

165 of the constant volume occupied by compartment M to the tissue volume (volume fraction). The

166 product $\gamma^M\, u_{wall}^M$ represents the volumetric solution outflow per unit tissue volume through the

167 boundary of compartment M.

168

169   Similarly, the volume-averaged continuity equations of the solute $'i'$ on the macroscopic scale

170 (equation 5) and microscopic scale (equation 6) govern the distribution of the molar concentration

171 of the solute [49, 50].

$$\boxed{\frac{\partial \overline{C}_i}{\partial t} = \overline{R}_i - \nabla.\overline{\mathbf{J}}_i} \tag{5}$$

$$\boxed{\frac{\partial \overline{C}_i^M}{\partial t} = \overline{R}_i^M - \nabla.\overline{\mathbf{J}}_i^M - \frac{\gamma^M}{\varepsilon^M} J_{i,wall}^M} \tag{6}$$

172   Where,

173 C_i^M is the molar concentration of species $'i'$ in the control volume $'M'$.

174 $\overline{R}_i^M$ refers to the volumetric metabolism reactions in which the substrate participates (see section

175 3 for more details).

176 $\mathbf{J}_i^M$ is the bulk flux of species $'i'$ within phase M, and is discussed in section 4.

177 $\frac{\gamma^M}{\varepsilon^M} J_{i,wall}^M$ represents the net outward molar flux of solute $'i'$ from control volume $'M'$ to its adjacent

178 compartments across the wall (discussed in sections 4 and 5)

179 **3. Reaction Mechanism (R_i):**

     Cellular reactions can occur within the control volume (R_i^M) or at the surface of a separating

wall ($R_{s,i}^{M-N}$), and can lead to the metabolism or transport of the substrate. In this study, three

commonly used approaches for modeling cellular reactions are outlined. These models include

the *mass action law* (equations 7a and 7b), the *Michaelis-Menten* (equation 8) and *Hill kinetics*

11

model (equation 9), which are given below:

$$
\boxed{
\begin{array}{c}
\textit{Mass Action Law :} \\[2mm]
n^{th} \textit{ order kinetics :} \quad \overline{R}_i^{\,M} = \prod_{i=1}^{j} K_i^M \left(\overline{C}_i^{\,M}\right)^{\nu_i} \\[4mm]
1^{st} \textit{ order kinetics :} \quad \overline{R}_i^{\,M} = K^M \overline{C}^{\,M}
\end{array}
}
\qquad
\begin{array}{c}
(7a) \\[6mm]
(7b)
\end{array}
$$

$$
\boxed{\textit{Michaelis} - \textit{Menten equation :} \quad \overline{R}_i^{\,M} = V_{max} \dfrac{\overline{C}_i^{\,M}}{K_m + \overline{C}_i^{\,M}}}
\qquad (8)
$$

$$
\boxed{
\begin{array}{c}
\textit{Hill kinetics :} \quad \overline{R}_i^{\,M} = V_{max}\theta \\[3mm]
\textit{where,} \quad \theta = \dfrac{C_L^{\eta_h}}{K_A^{\eta_h} + C_L^{\eta_h}}
\end{array}
}
\qquad (9)
$$

The law of mass action states that the rate of a reaction is proportional to the concentrations of its reactants and products taken to the power of their stoichiometric coefficient. Equation 7a represents the law of mass action for a reaction with j substrates, where K_i^M is the equilibrium constant coefficient for substrate $'i'$ in region M, $\overline{C}_i$ is the volume-averaged concentration of substrate $'i'$, and ν_i is the order of the reaction relative to substrate $'i'$ which has a negative value for reactants and a positive value for products. In some cases, especially for complex reactions, such as reversible, parallel, and series reactions, the reaction rate can be shown in the form of the first-order kinetic (equation 7b), in which the reaction rate and the substrate concentration has a linear relationship to each other [51, 52].

The Michaelis-Menten equation (equation 8) is one of the most effective methods for modeling single-substrate, single-product enzyme kinetics, and metabolic reactions. It relates the reaction velocity to the substrate concentration [53]. In the Michaelis-Menten equation, V_{max} represents the maximum velocity achieved by the system at the maximum (saturated) substrate concentrations, and K_m is the Michaelis-Menten constant, which represents the concentration of the substrate when the reaction velocity is equal to half the maximum velocity [54].

The Hill equation, (equation 9) is commonly used to describe the dependence between the binding of smaller molecules (*ligand*, such as ions) to macromolecules (such as proteins). The term θ in the Hill equation represents the fraction of macromolecules bound to the ligand. In obtaining θ, C_L is the concentration of free (unbound) ligand, K_A is the ligand concentration at which half-saturation (half-activation) is achieved, and η_h is the Hill coefficient. The Hill coefficient is also known as the interaction coefficient, and determines the extent of cooperativity between the ligand and the macromolecule binding sites [55, 56]. $\eta_h > 1$ represents positive cooperative binding, $\eta_h < 1$ represents negative cooperative binding, and $\eta_h = 1$ indicates a non-cooperative mechanism (completely independent binding processes). In the case of $\eta_h = 1$ the Hill equation reduces to the familiar Michaelis Menten model ($K_A = K_m$) [57].

4. Mass Transport Mechanisms:

The overall rate and type of material exchange within or across a compartment depend on the physical properties of the control volume and the structure of the separating wall, as well as the molecular features of the species being transported, such as their size, polarity, fat-solubility, diffusion coefficient, and the membrane partition coefficient for the solute.

Possible transport mechanisms "within" a control volume (e.g., M) are *convection*, *diffusion*, and *migration*, as follows:

$$\mathbf{J_i^M} = \mathbf{J}_{i,convection}^M + \mathbf{J}_{i,diffusion}^M + \mathbf{J}_{i,migration}^M \tag{10}$$

These mechanisms and the related equations are discussed in sections 4.1, 4.2, and 4.3, respectively.

Transport "between" the M and N domains occurs either through the gaps between the cells of the wall separating the domains or across the individual cell membranes (see Figure 2). Mechanisms of transport through gaps between the cells include *filtration* (section 4.1) and *diffusion* (section 4.2). Transport "across the cell membrane" can occur via diffusion, *ion channels* (section 5.1.1), *water channels* (section 5.1.2), *uniporters* (section 5.2.1), *pumps* (section 5.2.2), *symporters* (5.2.3), *antiporters* (section 5.2.4), and *cytosis* (see Figure 3).

13

The net outward molar flux across the $M - N$ interface $(J_i^{M,N})$ is given by:

$$\gamma^M J_{i,wall}^M = \sum_{N=1}^{m} \gamma^{M,N} J_i^{M,N} \tag{11}$$

Where m is the total number of adjacent control volumes. The mass transport mechanisms across the M-N wall can be grouped as follows:

$$J_i^{M,N} = \underbrace{J_{filtration} + J_{diffusion} + J_{ionchannel} + J_{waterchannel} + J_{uniporter}}_{\text{passive transport}} \\ + \underbrace{J_{pump} + J_{symporter} + J_{antiporter} + J_{cytosis}}_{\text{active transport}} \tag{12}$$

Where,

$J_{filtration}$ is the transported flux due to the hindered convection, and is discussed in section 4.1,

$J_{diffusion}$ is the transported flux due to the hindered diffusion, and is discussed in section 4.2,

$J_{ionchannel}$ is the ion flux through the ion channels, and is discussed in section 5.1.1,

$J_{waterchannel}$ is the water flux through the water channels, and is discussed in section 5.1.2,

$J_{uniporters}$ is the transported flux driven via uniporters, and is discussed in section 5.2.1,

J_{pumps} is the transported flux driven via pumps, and is discussed in section 5.2.2,

$J_{symporters}$ is the transported flux driven via symporters, and is discussed in section 5.2.3,

$J_{antiporters}$ is the transported flux driven via antiporters, and is discussed in section 5.2.4.

$J_{cytosis}$ is the transported flux driven via cytosis mechanisms, and is not discussed in this work.

Transport mechanisms can also be categorized as **passive** or **active** transport. Passive transport (filtration, diffusion, ion channel, water channel, and uniporter mechanisms) involves the spontaneous movement of the solutes, while active transport (pump, symporter, antiporter, and cytosis) requires an external source of energy. The following sections provide a detailed discussion of all these transport mechanisms except for cytosis, as the mechanism of cytosis is entirely different from the others.
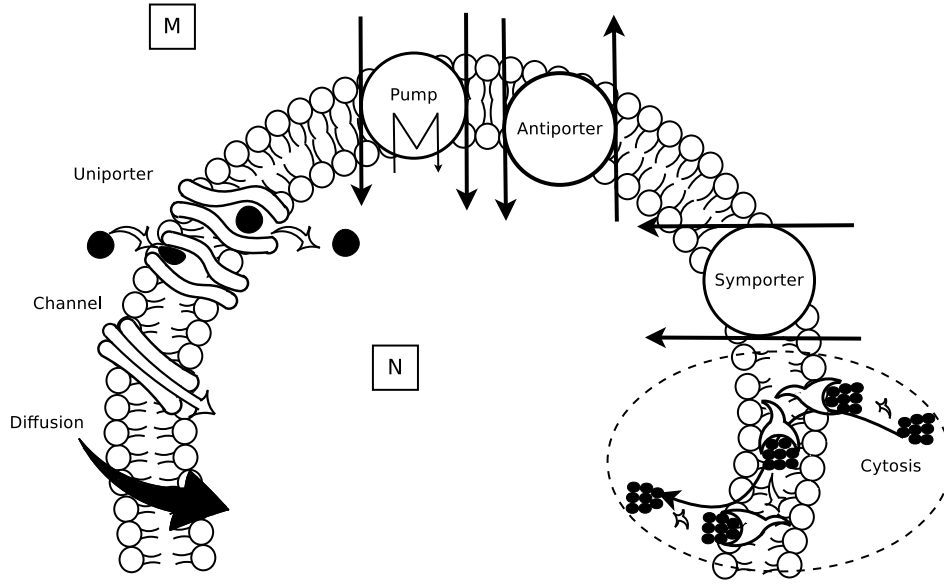
14

Figure 3: Transport across the cell membrane. Movement across the cell membrane can occur through channels, including *ion channels* (section 5.1.1) and *water channels* (section 5.1.2), *uniporters* (section 5.2.1), *pumps* (section 5.2.2), *symporters* (5.2.3), *antiporters* (section 5.2.4), and *cytosis*.

4.1. Convection and Filtration ($\mathbf{J_{convection}}$ and $\mathbf{J_{filtration}}$):

Convection is a mass transport mechanism that occurs due to the bulk motion of the fluid within a control volume and across the semipermeable porous wall. Fluid convection can be considered at two levels: (i) Internal flow convection ($\mathbf{u}^M$, $J^M_{i,convection}$), i.e., flow within the control volume, and (ii) filtration flow ($\mathbf{u}^{M-N}$, $J^{M-N}_{i,filtration}$), i.e., flow across the porous wall separating the compartments (Figure 4).
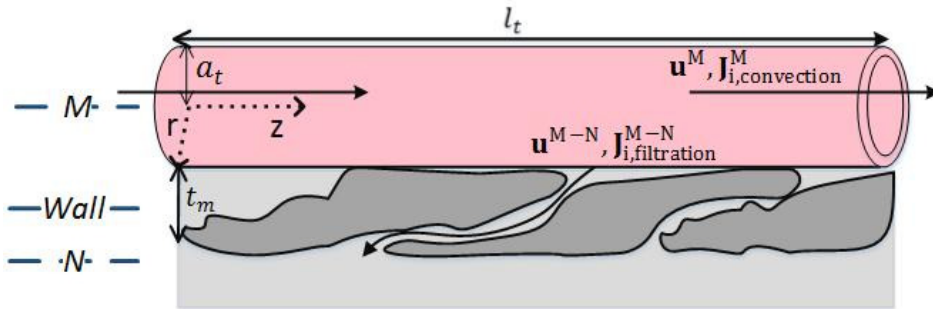

Figure 4: Convective flow inside the control volume ($\mathbf{u}^M$, $J^M_{i,convection}$) and filtration flow ($\mathbf{u}^{M-N}$, $J^{M-N}_{i,filtration}$) through the pores across the porous wall separating the compartments.

(i) Internal flow convection (M):

The Newtonian, laminar, and incompressible *fluid* flow inside a tube (control volume M) is governed by the Navier-Stokes and continuity equations (equations 3 and 4). A cylindrical tube whose length (l_t) is much larger than its radius (a_t) has no substantial radial pressure distribution, and consequently, no radial fluid movement. Under these conditions, the Poiseuille-Hagen Law relates the local "axial" fluid flow rate through a circular cross-sectional area of the tube to the hydrodynamic pressure difference at the two ends of the tube segment in the z-direction and the fluid viscosity by [58–60]:

$$F^M_{convection}(z, t) = -\frac{\pi a_t^4}{8\mu} \frac{\partial P^M}{\partial z} \tag{13}$$

Where $F^M_{convection}(z, t)$ is the axial volumetric flow rate in the tube per unit time (cm^3/s), $a_t = a_t(z, t)$ (cm) is the local radius of the tube, (μ) is the fluid viscosity $(Pa \cdot s)$, and $P = P(z, t)$ is the local axial pressure (Pa).

The axial fluid velocity within the tube ($u_z^M(r)$) through the total cross-sectional area of the tube is obtained by [50, 61]:

$$\boxed{Convection - fluid: \quad \mathbf{u}_z^M(r) = \frac{2F_{convection}}{\pi a_t^4}(a_t^2 - r^2) = -\frac{(a_t^2 - r^2)}{4\mu} \frac{\partial P^M}{\partial z}} \tag{14}$$

Where $u_z^M(r)$ is a function of the radial distance from the center of the tube ($0 < r < a_t$).

The convective flux of the *solute*, $J^M_{i,convection}$ $(mole/(s \cdot m^2))$, is coupled to the fluid velocity within the control volume M and the solute concentration, , C_i^M ($mole/m^3$), by [62, 63]:

$$\boxed{Convection - solute: \quad \mathbf{J}^M_{i,convection} = \mathbf{u}^M C_i^M} \tag{15}$$

(ii) Filtration-Transmembrane Flow (from M to N):

Filtration involves the passage of a hindered convective flow through a porous wall, and depends on the structure of the wall and the *effective pressure difference* between the two sides of the wall. The effective pressure drop ($\Delta P^{M,N}_{net}$) is the net result of the hydrodynamic pressure difference ($\Delta P^{M,N}$) and the osmotic pressure difference ($\Delta \pi^{M,N}$) between the two sides of the pore opening, and is given by equation 16a. The osmotic pressure difference is created by the solutes that are

retained from transport across the wall and is obtained through equation 16b [61, 64].

$$\Delta P_{net}^{M,N} = \Delta P^{M,N} - \Delta \pi_i^{M,N} \tag{16a}$$

$$\Delta \pi_i^{M,N} = RT \sum_{i=1}^{n} \sigma_i \Delta C_i^{M,N} \tag{16b}$$

Here, R is the universal gas constant (8.314 $J/(mol \cdot K)$), T is the temperature in Kelvin (human body temperature is around 300.98 K), and σ_i is the reflection coefficient. The reflection coefficient, which is also known as the osmotic coefficient, determines the real contribution of the osmotic pressure to the fluid flux through the membrane and is independent of the solute concentration and pressure.

The total volumetric filtration *fluid* flow rate through all the pores across the porous wall can be obtained by applying Poiseuille's Law, and is expressed as follows [61, 65–67]:

$$F_{filtration}^{M,N} = L_p A_s \Delta P_{net}^{M,N} \tag{17a}$$

$$L_P = \frac{\varepsilon a_p^2}{8\mu\tau t_m} = \frac{n''\pi a_p^4}{8\mu\tau t_m} \qquad where: \qquad \varepsilon = \frac{A_p}{A_s}, \qquad A_P = n\pi a_p^2 \qquad A_s = 2\pi a_t l_t \tag{17b}$$

Where L_p ($m/(s \cdot pa)$) is the filtration coefficient, A_s is the surface area of the tube, and $\Delta P_{net}^{M,N}$ is the effective pressure difference. The filtration coefficient, which is also known as hydraulic conductivity, determines the hydraulic permeability of the porous membrane to the fluid. The filtration coefficient can be obtained through equation 17b, where ε is the porosity of the wall and relates the actual available area of the heterogeneous porous membrane (A_p) to its total circumferential area (A_s), n is the number of non-uniform inert cylindrical membrane pores, n'' is the density of the pores across the membrane (n/A_s), a_p is the radius of the membrane pores, μ is the dynamic viscosity of the fluid, and τ is the tortuosity coefficient, which relates the actual available transport path to the membrane thickness, t_m [17]. In obtaining the total circumferential area (A_s), a_t and l_t are the radius and length of the tube, respectively.

The net outward filtrate fluid exchange velocity (filtration or ultrafiltration velocity) across the

17

membrane ($\mathbf{u}^{M,N}$) is given by [68]:

$$\boxed{Filtration - fluid: \quad \mathbf{u}^{M,N} = \frac{F_{filtration}^{M,N}}{A_s} = L_p(\Delta P^{M,N} - RT \sum_{i=1}^{n} \sigma_i \Delta C_i^{M,N})} \tag{18}$$

Equation 19 relates the macroscopic filtrate fluid flow velocity across the circumferential membrane area to its microscopic velocity in the membrane pores ($\mathbf{u}_{pore}^{M,N}$) [49].

$$\mathbf{u}_{pore}^{M,N} = (\frac{1}{\varepsilon}) \, \mathbf{u}^{M,N} = \frac{a_p^2}{8\mu\tau t_m} \Delta P_{net}^{M,N} \tag{19}$$

At the microscopic level, the non-steady state convective flux of the *solute* within the membrane pore ($J_{i,filtration(solute)}^{pore}$) is modified due to the restriction caused by the solute-membrane interaction, and is given by the expression [69]:

$$\mathbf{J}_{i,filtration}^{pore} = \beta_i^{pore} C_i^{pore}(y) u_{pore}^{M,N} \tag{20}$$

Where β_i is the restriction coefficient and depends on the interactions between the solute and the porous wall, and $C_i^{pore}(y)$ is the local concentration of the solute within the pore. The solute transport flux rate due to the hindered convection across the membrane from region M to N (also known as the solvent drag flux) is expressed as [70–73]:

$$\boxed{Filtration - solute: \quad J_{i,filtration}^{M,N} = \overline{C}_i^{M,N}(1 - \sigma_i) \, u^{M,N}} \tag{21}$$

$$where; \quad \overline{C}_i^{M,N} = \frac{C_i^M - C_i^N}{ln C_i^M - ln C_i^N}$$

Where $\overline{C}_i^{M,N}$ is the logarithmic mean average of the concentrations at the two sides of the membrane and $(1 - \sigma_i)$ represents the fraction of the solute dragged across the membrane by the fluid flow.

*4.2. Diffusion (**J**_{diffusion}):*

Diffusion transport flux moves substances passively from a higher concentration region to lower concentration. Similarly to convection, diffusion can be considered at two levels: (i) diffusion within the region (e.g., M), known as *free diffusion*, and (ii) diffusion across the membrane separating the regions (e.g., between M and N), which is known as *restricted diffusion*.

(i) Diffusion-within the region (free diffusion): The partial differential form of Fick's law below can be used to determine the free diffusive flux [74]:

$$\mathbf{J}_{i,diffusion}^{M} = -D_i^M \nabla C_i^M \tag{22}$$

Where D_i^M is the free diffusion coefficient for species $'i'$ in the control volume M, and has the unit (cm^2/s). Depending on whether the molecule is charged or uncharged, D_i^M obtained using equations 23, 24, and 25a, respectively.

The diffusion coefficient for an uncharged solute in a dilute liquid solution can be calculated either by applying the *Wilke − Chang* method (equation 23) [45, 75, 76] or the *Stokes − Einstein* method (equation 24) [49, 67, 77].

$$Wilke - chang: \quad D_{i,uncharged}^M = 7.4 \times 10^{-15} \frac{T \sqrt{\varnothing_w M_w}}{(\sum \hat{v}_s)^{0.6} \mu} \tag{23}$$

$$Stokes - Einstein: \quad D_{i,uncharged}^M = \frac{K_B T}{6\pi a_s \mu} \tag{24}$$

Where T is the temperature in Kelvin, $\varnothing_w$ is the solvent association factor, M_w is the molecular weight of the solvent, $\hat{v}_s$ is the molar volume of the solute, and μ is the solvent viscosity, a_s is the radius of the spherical particle, and K_B is the Boltzmann's constant $(1.38 \times 10^{-23} \ m^2 \cdot kg/(s^2 \cdot K))$. The free diffusion coefficient for a charged particle can be obtained from the expression [49]:

$$D_{i,charged}^M = \left(\frac{RT}{F^2}\right) \frac{\Lambda_i^\infty}{|z_i|} \tag{25a}$$

Where R is the universal gas constant $(8.314 \ J/(mol \cdot K))$, z_i is the ionic charge, F is Faraday's constant $(96, 490 \ A \cdot s/mol)$, Λ_i^∞ is the electrical conductance of ion $'i'$ in the solution $(m^2/(ohm \cdot eq))$.

(ii) Diffusion-through the membrane (restricted diffusion): The one-dimensional restricted diffusion flux rate of a solute through a thin semipermeable membrane can be determined using Fick's equation as below:

$$J_{i,diffusion}^{pore} = -D_{i,eff}^m \frac{\partial C_i}{\partial y} \qquad (26)$$

Where $D_{i,eff}^m$ is the *effective* diffusion coefficient of the solute in the membrane. The effective diffusion coefficient, also known as the restrictive diffusion coefficient, determines the effect of the heterogeneity and tortuosity of the biological membrane on the diffusion rate and is given by the expression [51, 69, 78]:

$$D_{i,eff}^m = \frac{\beta_i^m}{\tau^m} D_i^m \qquad (27)$$

Where β_i^m and τ^m are the solute restriction coefficient and tortuosity coefficient of the membrane layer, respectively.

The diffusive flux equation can be obtained in terms of the membrane permeability coefficient P_i^m (cm/sec) by integrating the differential form of Fick's equation over the membrane thickness, t_m (cm). [47, 79]:

$$J_{i,diffusion}^{M,N} = P_i^m (C_i^M - C_i^N) \qquad (28)$$

Where $J_{i,diffusion}^{M,N}$ has the unit of number of molecules per unit area per unit time. Permeability (P_i^m) is a phenomenological coefficient that relates the diffusion flux to the concentration gradient across the two sides of the membrane. The permeability of the porous membrane towards a molecule is usually determined experimentally; however, it can also be obtained theoretically using equation 29 [80].

$$P_i^m = \frac{K_i^m}{t_m} D_{i,eff}^m \qquad (29)$$

256   Where K_i^m is the membrane partition coefficient for solute $'i'$.

257   *4.3. Migration (**J**$_{migration}$):*

The distribution of ions within a control volume or across the membrane can generate an electric field (**E**, (V/m)). The produced electric field exerts an external force on charged particles,

20

causing them to move either with or against the diffusive transport flux. This type of transport is known as *migration* and the migrative flux is obtained using the expression below [47, 49, 81, 82]:

$$\boxed{\mathbf{J}^{\mathbf{M}}_{\mathbf{i,migration}} = \mathbf{E}\nu_i^M(C_i^M)} \tag{30}$$

Where ν_i^M, and C_i^M are the electrokinetic mobility $(m^2/(s \cdot V))$ and concentration of the ion, respectively. The single ion mobility (ν_i^M) and the diffusion coefficient (D_i^M) are related by the expression:

$$\nu_i^M = \frac{D_i^M z_i F}{RT} \tag{31}$$

Where z_i is the valence of the ion, F is the Faraday's constant $(96,490\ A \cdot s/mol)$, R is the universal gas constant $(8.314\ J/(mol \cdot K))$ and T is the temperature in Kelvin.

The relationship between the electrical field (mV/cm) and the electric potential (mV) are given by:

$$\mathbf{E} = -\nabla\psi_E \tag{32a}$$

$$\nabla\psi_E^{M-N} = V_m^{M-N} = \psi^M - \psi^N \tag{32b}$$

Where $\nabla\psi_E$ is the electrical potential gradient. The electrical potential gradient across the two sides of a thin membrane, which is known as the membrane voltage $(V_m^{M,N})$, can be obtained by using equation 32b.

5. Membrane mediated transport mechanisms:

After discussing the three main mass transport mechanisms, convection (filtration), diffusion, and migration, this section deals with transport across the membrane, which can be mediated via specific groups of integrated membrane proteins known as **transporters** [83]. Transporters are the class of membrane proteins including channels (ion channels and water channels), pumps, carrier-mediated proteins (uniporters, symporters, antiporters), and receptor-mediated transporters. These membrane proteins play a crucial role in maintaining the electrochemical gradient across the cell membrane, the uptake of nutrients, drug transport, and the removal of cell metabolism waste products [84, 85]. For further details on the structure of these transporters, their molecular mechanisms, and their application in drug transport, please refer to references [26, 86–94].
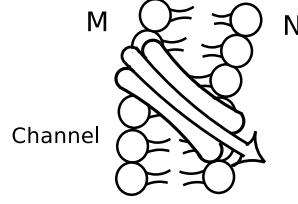
*5.1. **Channels** (**J**ionchannel , **J**waterchannel):*

Figure 5: Channel Transport Mechanism

The lipid bilayer membrane of the cell is impermeable to highly charged and hydrophilic molecules, such as ions and water molecules. However, the cell membrane contains solute-specific proteins known as channels that allow water molecules and charged substances to diffuse or migrate through them [26, 95]. Some of these channels are mainly permeable to ions, and are thus called ion channels, while those that are permeable to water molecules are known as water channels or aquaporins.

*5.1.1. Ion Channel (**J**ionchannel) :*

Ion channels create pathways for the passive movement of charged, hydrophilic molecules by diffusion and migration mechanisms. Various mathematical models can be used for the ion flux through ion channels. In order for these models to be precise, the size of the ion, possible reactions among the ions in the pathway, and interactions of the wall of the protein channel with the ion being transported should be considered [40, 96–98]. Here, the ion channel models are classified depending on their scale as (i) ion distribution *within (inside)* the channel (ii) the *net driven* ion flux through the ion channels from one side (M) of the membrane containing the ion channels to the other (N).

(i) Ion flux within (alongside) the channel: The total ion flux within a channel is commonly modeled using a modified form of the Nernst-Planck equation. The Nernst-Planck equation gives the total ionic flux as the balance between the diffusive flux (equation 22) and the electrical drift (equation 30) and can be written as below [81, 96, 99]:

$$\mathbf{J_i^{ion\ channel}} = -D_i^m \left(\nabla C_i + \left(\frac{z_i F}{RT} \right) C_i \nabla \psi_i^{eff} \right) \tag{33}$$

Where D_i^m is the ion diffusion coefficient and can be obtained theoretically using equation 25a, and $\nabla \psi_i^{eff}$ is the effective potential, which depends on the electrostatic potential and the interactions between transferring ions and the channel wall.

The one-dimensional volume-averaged ion flux over the cross-sectional area of the channel can be given as [49]:

$$\overline{\mathbf{J_i}}^{\text{ion channel}} = -D_{i,eff}^m \left(\frac{d\overline{C_i(y)}^{ion\ channel}}{dy} + \left(\frac{z_i F}{RT}\right) \overline{C_i}^{ion\ channel} \frac{d\psi_i^{eff}(y)}{dy} \right) \tag{34}$$

Where $D_{ion,eff}^m$ is the restrictive diffusion coefficient for the ion and can be obtained by applying equation 25a in equation 27.

The one-dimensional form of the Poisson equation (equation 35) relates the spatial electric field distribution to the local charge density ($\sigma(y)$) via the expression below [49]:

$$\sigma(y) = -\varepsilon_0 \frac{d^2 \psi^{eff}}{dy^2} = F \sum_{i=1}^{m} z_i \overline{C_i(y)}^{ion\ channel} + \sigma_p(y) \tag{35}$$

Where ε_0 is the dielectric constant (electrical permeability), the expression "$F \sum_{i=1}^{m} z_i \overline{C_i(y)}^{ion\ channel}$" sums the charge density on each of the $'m'$ individual ions, and $\sigma_p(y)$ is the charge density on the immobilized protein wall of the membrane channel.

The combination of equation 34 with equation 35 is known as the Poisson-Nernst-Planck (PNP) model, and can be used develop a full model of ion distribution along the ion channels [96].

(ii) Net driven ion flux through the channel: The net ion flux from region M to N through the channel ($mol/cm^2 \cdot s$) is related to the current across the membrane (A/cm^2) by the expression[100]:

$$\boxed{J_{i,ion\ channel}^{M,N} = \frac{I''_{i,channel}^{M,N}}{z_i F}} \tag{36}$$

Where $I''_{i,channel}^{M,N}$ is the net current density of ion $'i'$ through $n_{i,channel}$ channels sensitive to ion $'i'$, and is given by the expression:

$$I''_{i,channel}^{M,N}(V_m,t) = n''_{i,channel}\, f_o^{i,channel}(V_m,t)\ i_{i,channel}^{M,N}(V_m,t) = O_i^{channel}(V_m,t)\, i_{i,channel}^{M,N}(V_m,t) \tag{37}$$

Where $n''_{i,channel}$ is the ion channel density per unit area of the membrane, $f_o^{channel}(V_m,t)$ is the probability that the ion channel is in open state at time t and has a value between 0 and 1 ($0 \leq f_o^{channel} \leq 1$).

Most of these channels are not always open, and can be switched between at least two states

23

$_{301}$ (the open and closed states) in response to a chemical, electrophysiological, or hormonal stimulus.

$_{302}$ The probability that the channel will be open is a function of the membrane potential (V_m) and

$_{303}$ the channel structure; the product $n''_{i,channel} f_o^{i,channel}$ is sometimes denoted by a single variable,

$_{304}$ $O_i^{channel}$, which refers to the total number of open channels per unit area of the membrane (A_m)

$_{305}$ (# of channels/cm^2). Details of the types of gating are beyond the scope of this work. For further

$_{306}$ details, one can refer to references [87], [26], and [101–104].

$_{307}$ $i_i^{M,N}(V_m, t)$ is the current driven across the membrane through one channel (from region M to N).

$_{308}$ The ion current through the lipid bilayer membrane be modeled in two ways: using the Ohm model

$_{309}$ (equation 38) or the Goldman-Hodgkin-Katz (GHK) model (equation 41).

Ohm model: The current through a gating channel ($i_{i,OhmChannel}^{,M,N}$) according to Ohm's law is given by the expression below [102, 105]:

$$i_{i,Ohm}^{M,N} = g_{i,channel}(V_m, C, t)\left(V_m^{M,N} - V_{i,rev}^{M-N}\right) \tag{38}$$

Where $g_{i,channel}$ (V_m, C, t) is the membrane conductance for channels of ion $'i'$ (channel conductance) in units of Siemens ($S = 1/Ohms$) and can be a function of membrane voltage (V_m), ion concentration (C) and time (t), $V_m^{M,N}$ is the membrane voltage (equation 32b), and $V_{i,rev}^{M-N}$ is the membrane reversal potential for a single ion $'i'$. At equilibrium, there is a balance between the electrical and chemical forces, and consequently, there is no net ionic flux across the membrane; otherwise, the membrane potential will vary and produce an electric field across the membrane, which in turn produces an ion flux across the membrane. The membrane potential, which is also known as the equilibrium or resting potential, at the equilibrium state (zero current) is known as the reversal potential, and can be calculated for a particular charged ion $'i'$ using the *Nernst-potential* equation below:

$$V_{i,rev}^{M-N} = -\frac{RT}{z_i F} ln\left(\frac{C_i^{M(in)}}{C_i^{N(out)}}\right) \tag{39}$$

The overall current flux (per unit area of the membrane) of the individual ion $'i'$ using the Ohm

model is given below:

$$
\boxed{
\begin{aligned}
Ohm\ \ &current\ \ model: \\
I''^{M,N}_{i,Ohmchannel} &= n''_{i,channel} f^{i,channel}_o(V_m, t)\ g_{i,channel}\left(V_m - V^{M-N}_{i,rev}\right) \\
&= O^{channel}_i(V_m, t)\ g_{i,channel}\left(V_m - V^{M-N}_{i,rev}\right)
\end{aligned}
}
\tag{40}
$$

Goldman-Hodgkin-Katz current model: If the ion channel is sufficiently short, and the charge density of the protein channel does not exceed the ion charge density, the right-hand side of the Poisson equation (equation 35) becomes zero. These assumptions lead to a fixed electric potential and electric field across the membrane ($d\psi/dy = -\psi^m/t_m$). The *Goldman-Hodgkin-Katz* (*GHK*) model approximates the ionic flux across the membrane through a given ion channel by assuming a constant electric field across the membrane. The GHK equation for outward ion current across the membrane from M to N is written as [106]:

$$
i^{M,N}_{i,GHK} = P^{M-N}_i \frac{z_i^2 F^2 V^{M-N}_m}{RT} \frac{C^M_i - C^N_i exp\frac{-z_i F V^{M-N}_m}{RT}}{1 - exp\frac{-z_i F V^{M-N}_m}{RT}}
\tag{41}
$$

Where P^{M-N}_i, which has units of $(cm/(pore \cdot s))$, is the membrane permeability towards the specific ion $'i'$ through a single pore, and determines the amplitude of the membrane conductance for that ion.

The overall individual ionic current carried by ion $'i'$ per unit area of the membrane can be calculated using the GHK model as [102, 107]:

$$
\boxed{
\begin{aligned}
Goldman &- Hodgkin - Katz\ \ current\ \ model: \\
&I''^{M,N}_{i,GHKChannel} = \\
n''_{i,channel} f^{i,channel}_o P^{M-N}_i &\frac{z_i^2 F^2 V^{M-N}_m}{RT} \frac{C^M_i - C^N_i exp\frac{-z_i F V^{M-N}_m}{RT}}{1 - exp\left(\frac{-z_i F V^{M-N}_m}{RT}\right)} = \\
O^{channel}_i P^{M-N}_i &\frac{z_i^2 F^2 V^{M-N}_m}{RT} \frac{C^M_i - C^N_i exp\frac{-z_i F V^{M-N}_m}{RT}}{1 - exp\left(\frac{-z_i F V^{M-N}_m}{RT}\right)}
\end{aligned}
}
\tag{42}
$$

310 *5.1.2. Water Channel (*$\mathbf{J_{waterchannel}}$*):*

The small polar and uncharged molecule water can move across the cell membrane by the simple diffusion mechanism. However, the diffusion of water through the lipid membrane is rela-

tively slow; therefore, additional pathways for the movement of water across the membrane must exist. Recent studies have shown that the cell membrane contains water channels, known as *Aquaporins* (AQP), that allow the passage of lipophobic water molecules through the cell membrane [83, 108, 109]. These channels play a crucial role in regulating the cell volume as well as in pathological conditions [110, 111]. More details about the discovery and various types of water channels and their structure, regulation, and distribution in different cell and tissue types in the body can be found in references [112] and [113–115]. The water flux through the water channels can be expressed as [100, 116–118]:

$$J_{waterchannel}^{M,N} = L_{water,p}^{AQP}(\Delta P_{hydraulic}^{M,N} - \sum_i \sigma_i^{MN} \Delta \pi_i^{M,N} - \sigma_p \Delta \prod_{p,oncotic}^{M,N}) \tag{43}$$

Where $L_{water,p}^{AQP}$ is the hydraulic conductivity of the membrane towards water, $\Delta P_{hydraulic}$ is the hydraulic pressure difference, $\Delta \pi_{osmosis}$ is the osmotic pressure difference (equation 16b), and σ_i is the reflection coefficient, which determines the real contribution of the osmotic pressure to the driven water flux through these channels. $\Delta \prod_{p,oncotic}$ is the oncotic or colloid osmotic pressure difference, which corresponds to the osmotic pressure created by high-molecular-weight plasma proteins. The oncotic pressure difference can empirically be determined using the Landis and Pappenheimer model (equation 44) [119–121]:

$$\prod_{oncotic,total}^{M} = 2.1 \, C_{protein}^{M} + 0.16 \, (C_{protein}^{M})^2 + 0.009 \, (C_{protein}^{M})^3 \tag{44}$$

Where $\prod_{oncotic,total}^{M}$ is the plasma colloid osmotic pressure, and $C_{protein}^{M}$ is the total plasma protein concentration within the region M (grams of protein per 100 liters of solution).

5.2. *Carrier-Mediated Transport* ($J_{uniporter}$, J_{pump}, $J_{symporter}$, $J_{antiporter}$):

Some lipid-insoluble substances have low permeabilities across the cell membrane, or are too large to enter the cell via filtration and diffusion mechanisms or move through membrane channels and pores. Moreover, in some situations, a cell must import a solute against the direction of the electrochemical gradient to meet its needs. In these scenarios, the relevant solute may cross the membrane via membrane-integrated proteins known as *carriers*; the corresponding transport mechanism is known as *carrier-mediated transport*. Similarly to channels, these transporters are highly solute-specific; however, unlike channels, they do not contain hydrophobic pores. There-

26

fore, carriers can only bind to one or a few substrate molecules at a time, and transport via carriers is much slower than via channels. Carrier-mediated transport is a multi-step process. Its underlying mechanism is briefly addressed below and schematically depicted in Figure 6. In the first step, the substrate being transported (ligand) participates in a reversible binding (association) reaction with the binding site of the carrier on one side of the membrane (see Figure 6-b and 6-c). After the carrier-substrate complex has been formed, the carrier undergoes a conformational change and translocates the substrate across the membrane. Finally, the carrier releases the substrate at the other face through a dissociation reaction. Energy is needed to achieve the conformational change; depending on the source of the energy, the carrier is categorized as a **uniporter**, **pump**, **symporter**, and **antiporter**.

a

b

M-Side N-Side
Association Translocation Dissociation
E A

$$E_M + A_M \underset{k_{A_M}^-}{\overset{k_{A_M}^+}{\rightleftharpoons}} EA_M \qquad EA_M \underset{g_{EA}^N}{\overset{g_{EA}^M}{\rightleftharpoons}} EA_N \qquad EA_N \underset{k_{A_N}^+}{\overset{k_{A_N}^-}{\rightleftharpoons}} E_N + A_N$$

Flow Chart Key

A — Ligand

— Carrier

A — Carrier-Ligand Complex

M-Side

$$E_M + A_M \overset{K_A^M}{\rightleftharpoons} EA_M$$

$$E_M \underset{g_E^N}{\overset{g_E^M}{\rightleftharpoons}} E_N \qquad EA_M \underset{g_{EA}^N}{\overset{g_{EA}^M}{\rightleftharpoons}} EA_N$$

$$E_N + A_N \underset{K_A^N}{\rightleftharpoons} EA_N$$
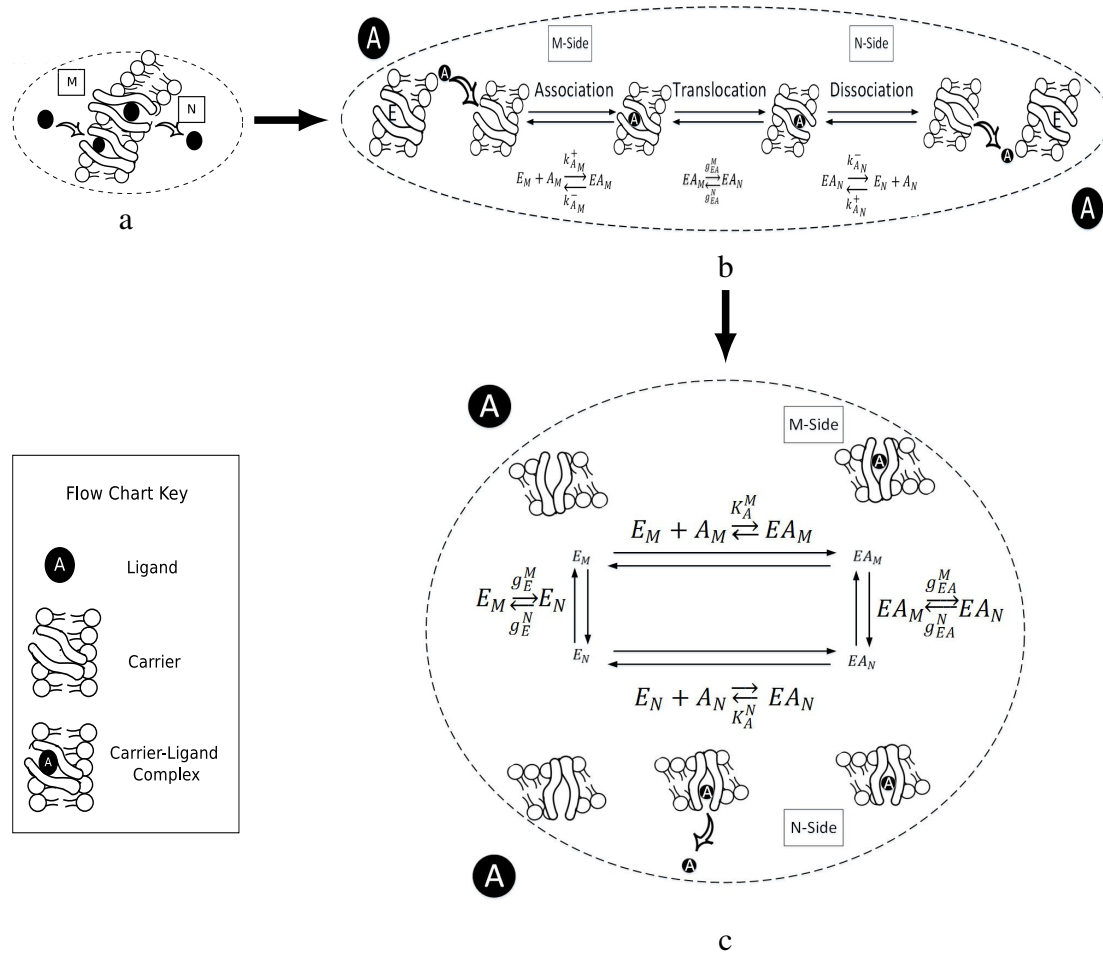
N-Side

c

Figure 6: A possible process by which a carrier protein can mediate the transport of a solute molecule across the lipid bilayer membrane. Figure *a* represents a uniporter (E), which transports a single solute (A) from one side of the membrane (M) to the other (N). Figures *b* and *c* represent the step-wise transport mechanism of solute (or ligand) *A* from one side of the membrane to the other side, besides the corresponding kinetic terms. First, the ligand binds the carrier on one side of the membrane (M) to form a EA_M complex; next, this complex passes the ligand across the membrane through a translocation step (carrier conformational shift) and then dissociates at the N side of the membrane. In Figure *b*, k_A^{+M} and k_A^{-M} are the association and dissociation rates, and superscripts show the side of the membrane that the reaction is taking place (sides M or N of the membrane). g_{EA}^M and g_{EA}^N are the carrier-ligand translocation rate constants with superscripts representing the side of the membrane translocation originates in (e.g., g_{EA}^M is the translocation rate constant from M side to N side of the membrane). In Figure *c*, K_A^M is the dissociation equilibrium constants and is defined as $K_A^M = k_A^{-M}/k_A^{+M}$. Moreover, in Figure *c*, there are two cycles: the inner cycle represents the forward substrate transport (influx); the outer cycle represents the backward flux (efflux).

The uniport transport mechanism is a *passive* transport mechanism, as the carrier facilitates the downhill movement of a single group of specific large polar molecules across the membrane, such as glucose and amino acids, which cannot easily penetrate the membrane. For this reason, transport

through uniporters is often referred to as "*facilitated diffusion*", in the sense that the membrane transporter facilitates the transport driven by the concentration gradient between the two regions (e.g., M and N) [122, 123]. However, it differs from other passive transport mechanisms (diffusion, migration, convection, and channels) as the solute participates in a series of biochemical reactions with the fixed membrane carrier to cross the membrane [122, 124, 125].

Active transport mechanisms are typically used by cells to transport components against the electrochemical gradient. For this movement to take place, an additional source of energy is needed. This extra energy can be supplied by coupling the transport of the solute to another cellular reaction or transport phenomenon. Depending on the source of the supplied energy, the transport mechanism can be classified as *Primary active transport* or *Secondary active transport* [17, 126, 127].

In primary active transport, the cell directly utilizes chemical energy stored in chemical bonds, which is mainly released by the hydrolysis of adenosine triphosphate molecules or an equivalent high-energy phosphoryl bond. Adenosine triphosphate, which is abbreviated as *ATP*, is known as the energy molecule of the cell. ATP molecules can release a large amount of energy via their conversion to adenosine diphosphate (*ADP*) and the release of a phosphate (P_i) ion group (ATP $\rightleftharpoons$ ADP + P_i). ATPase is the enzyme that catalyzes the ATP dephosphorylation reaction. For this reason, this family of transporters is commonly known as *"ATPase pumps"* and/or *ATP powered pumps* [95, 125, 128].

Secondary active transport mechanisms couple the electrochemical potential produced across the membrane during the transport of one group of components to the simultaneous uphill transport of another group of substances [129, 130]. The required electrochemical energy can be obtained from the simultaneous downhill transport of another family of solutes by the same transporter, or it can be exerted by the indirect involvement of the ATP hydrolysis reaction during the primary active transport of the other substrates. Cotransporters are capable of transporting two or more different families of solutes, and secondary active transporters can be further categorized as *symporters* and *antiporters*. The transport mechanism in which both types of solutes move in the same direction relative to each other is called symport transport, whereas the mechanism in which the solutes move in opposite directions is referred to as antiport transport.

The approach taken in developing the mathematical model of the transported flux driven via carriers differs from the ones discussed in earlier sections of this work. Since these transporters are embedded in the phospholipid bilayer membrane, they cannot diffuse across the membrane. Therefore, in the mathematical equations related to the carrier transport mechanism, there is no term associated with the diffusion coefficient, and the thermal behavior of the molecules is captured in the reaction rate coefficients. Consequently, to develop a quantitative model of the flux transported by each transporter, one must know the rate expression of all steps, including the association and dissociation constants for the reaction steps occurring on the membrane surfaces, as well as the translocation rate constants for translocating the unloaded and loaded carriers. The rate constants for the binding and unbinding of solute A on the surface of the membrane can be determined experimentally, and are $k_{A_M}^+$ and $k_{A_M}^-$, respectively for the M side; the equivalent values for the N side are $k_{A_N}^+$ and $k_{A_N}^-$ (Figure 6-b) [131]. The translocation rate of the transporter (denoted as g_E, g_{EA}, etc.) determines the number of molecules that the transporter can transport per one molecule of the carrier. The translocation rate constants are a function of the membrane permeability (P) to the transporter in addition to the total available number of transporters ($[E]_t$) and have units of inverse seconds ($1/s$) ($g = P[E]_t$). The carrier translocation rate constants and the total amount of the carrier are experimentally determined.

The kinetic models for each individual carrier differ from one another with respect to some details of their mechanisms and the solute transported. For some of these transporters to translocate the solutes, the binding and unbinding of each of the solutes must occur in a particular order. Furthermore, in some cases, several substances (competitors) compete with the solutes being transported during each translocation cycle for the same binding sites on the carrier. To reduce the modeling complexity of the transport mechanisms while still obtaining accurate prediction of the transported fluxes, one can make appropriate simplifying assumptions. The *rapid equilibrium* and *quasi-steady-state* assumptions are commonly used assumptions that are applied to most of the models discussed in this paper. Another assumption that is occasionally used is the *carrier symmetric assumption*. Each of these assumptions is discussed in more detail below. In the "rapid equilibrium assumption", the surface binding and unbinding reactions are assumed to occur much faster than the translocation of the complexes between the two sides of the membrane. That is, the

30

rate-limiting step of the transport cycle is the translocation of the carrier-solute complexes from one side of the membrane to the other. The rapid equilibrium assumption allows the concentrations at the membrane surfaces to be determined by assuming that the equilibrium constant coefficients are independent of the reaction path (e.g., in Figure 6-b and 6-c, $K_A^M = \frac{k_{A_M}^-}{k_{A_M}^+} = \frac{[A]_M[E]_M}{[EA]_M}$ for side M, and $K_A^N = \frac{k_{A_N}^-}{k_{A_N}^+} = \frac{[A]_N[E]_N}{[EA]_N}$ for the other surface) [131].

In the "quasi-steady-state", it is assumed that due to the high affinity of the substrates with respect to the carrier, the concentration of the intermediate complex does not change on the time scale of carrier production rate, and the total number of carriers per unit area of the membrane ($[E]_t$) is conserved during each cycle (i.e., in Figure 6, $[E]_t \ll [A] \Rightarrow \frac{d[EA]}{dt} = 0$).

In the "carrier symmetry assumption," the dissociation constants on both sides of the membrane are the same (e.g., $K_A^M = K_A^N = K_A$ in Figure 6-c) and that the backward and forward translocation reactions of the carrier occur at the same speed (e.g., in Figure 6, $g_{EA}^M = g_{EA}^N = g_{EA}$ and $g_E^M = g_E^N = g_E$).

In the remainder of this work, detailed studies of each carrier group and several well-known kinetic models are presented. Furthermore, for each carrier, a simplified model and its simplifying assumptions are outlined. Subsequently, following the kinetic parameterization of Stein (2012) [131], all models are transformed into a general identical resistance parametric form. Each model includes a figure that demonstrates a possible kinetic model in the left panel, while the right panel depicts a related sequence of reaction equations that address the transport mechanism by the carrier (e.g., see Figure 8). In each scheme, there are two cycles: the inner cycle represents the forward transport of substrates (influx); the outer cycle represents backward flux (efflux). The corresponding net flux of the carriers driven across the membrane is expressed as $J_{carrier}^{M,N(net)} = J_{carrier}^{M,N} - J_{carrier}^{N,M}$.

31

5.2.1. Uniporter Mechanism (J$_{Uniporter}$):
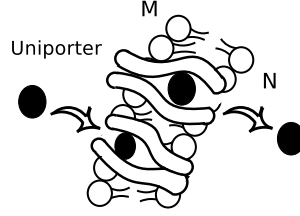
Figure 7: Uniporter Transport Mechanism

Figure 8 shows a possible reaction cycle for a uniporter (E) that can face the M side of the membrane, where it binds to solute A to form the complex EA_M. Next, the carrier-substrate complex translocates across the membrane with a translocation rate constant g^M_{EA} to face the other side of the membrane (EA_N). In the last step, the loaded carrier (EA_N) undergoes a dissociation reaction that releases substrate A at the N side of the membrane. The translocation of the free carrier, E_M and E_N, takes place with translocation rate constants of g^M_E and g^N_E, respectively. Stein (2012) [131] developed this model using the following assumptions: 1) the binding and unbinding reactions of the solute are rapid relative to the translocation step, 2) the quasi-steady-state assumption is valid, and 3) the carrier is non-symmetric; therefore, distinct equilibrium constants (K^M_A and K^N_A) and different translocation constants (g^M_E, g^M_{EA}, g^N_E, g^N_{EA}) are considered. The net turnover rate of the uniporter and the flux of molecules of A transported through the uniporter from side M to side N of the membrane can be obtained using equations 45 and 46, respectively.

32
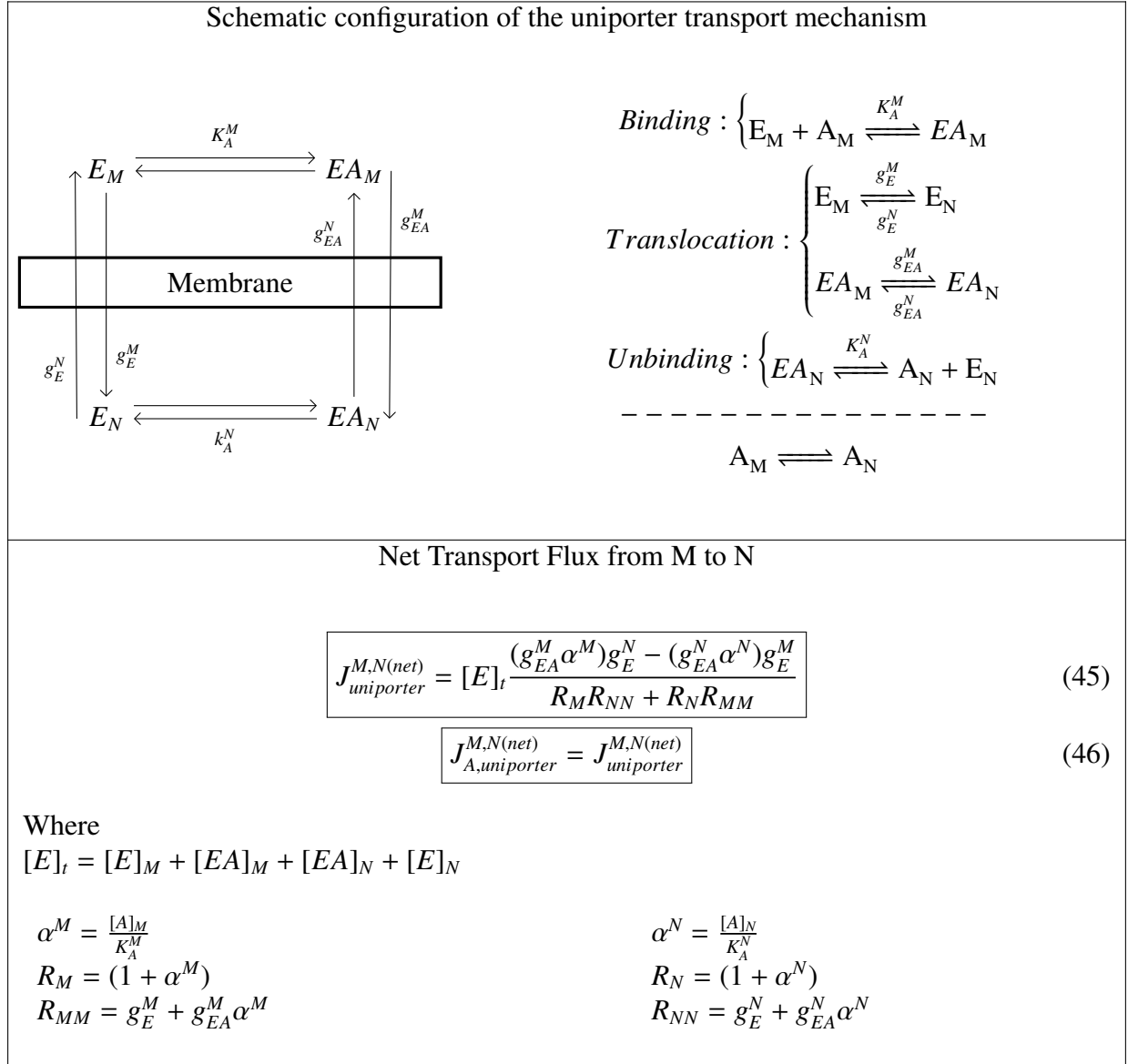
Figure 8: A schematic configuration of the uniporter transport mechanism and the regarding net flux transport equation. Dissociation constants (K_A^M, K_A^N) and the translocation rate constants (g_E^M, g_{EA}^M, g_E^N, g_{EA}^N) are depicted in the reaction cycle in the right panel. $[E]_t$ is the total number of transporter per unit area of the membrane. The flux equation is transformed to the general form of the resistance parameters from Stein model [131].

Uniporter simplified model:

If one invokes the symmetric assumption for the dissociation constants (i.e., $K = K_A^M = K_A^N$), three different cases can be considered depending on the relative value of the translocation rate constant of the free carrier constant to that of the carrier-ligand complex (g_E to g_{EA}) in addition to the solute concentration at the N side ($[A]_N$) relative to the dissociation constant (K). The "one-way" solute

flux for each case is expressed as below [49]:

case # 1) $g_{EA} \gg g_E$ and $[A]_N \geq K$: In this situation, an increase in $[A]_N$ leads to a higher transporter flux ($J_{uniporter}^{M,N}$):

$$J_{uniporter}^{M,N} = [E]_t g_{EA} \frac{[A]_M}{[A]_M(2 + \frac{K}{[A]_N}) + K} \tag{47}$$

case # 2) $g_{EA} \ll g_E$ and $[A]_N \leq K$: In this situation, increases in $[A]_N$ cause the transporter flux ($J_{uniporter}^{M,N}$) from M to N to fall, and vice versa:

$$J_{uniporter}^{M,N} = [E]_t g_{EA} \frac{[A]_M}{[A]_M(1 + \frac{[A]_N}{[A]_M}) + 2K} \tag{48}$$

case # 3) $g_{EA} = g_E$: The turnover of the loaded and unloaded carriers occurs at the same rate. In this case, when the concentration of the substrate is much higher than the availability of the carrier, the one-way flux of the solute from the M membrane surface to the N side will be:

$$J_{uniporter}^{M,N} = \left(\frac{[E]_t g_{EA}}{2} \right) \frac{[A]_M}{K + [A]_M} \tag{49}$$

Equation 49 is identical to the single-substrate enzymatic Michaelis-Menten reactions on the surface of the membrane and describes the rate of uptake of the substance as:

$$\boxed{J_{uniporter}^{M,N} = V_{max} \frac{[A]_M}{K_m + [A]_M}} \tag{50}$$

Where V_{max} and K_m are the Michaelis-Menten parameters. The maximum velocity (V_{max}) occurs when the solute concentration reaches infinity starting from an initial value of zero, and corresponds to the number of available sites on the carrier for substance uptake. Comparing equations 49 and 50, the maximum velocity of the reaction is $V_{max} = \frac{[E]_t g_{EA}}{2}$. $K_m = K$ is the half-saturation rate constant and represents the concentration of the substrate at which the half-maximal rate is observed. The half-saturation rate constant also determines the number of carrier turnovers and, consequently, the number of molecules of the solute transported by the carrier per unit time by each translocation of the solute-carrier complex.

*5.2.2. Primary active transport mechanism (**J**$_{\text{pump}}$):*
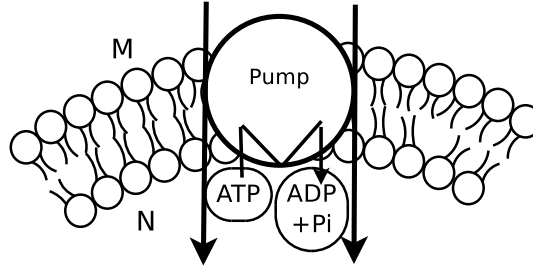
Figure 9: ATPase Transport Mechanism

ATPase pumps use the energy released during ATP hydrolysis to pump one or more groups of ions and molecules against an uphill electrochemical gradient. The net result of the step-wise uphill transport of one substance (A) via an ATPase pump is summarized in the following reaction equation:

$$A_N + (ATP)_N \rightleftharpoons A_M + (ADP)_N + (Pi)_N$$

As is clear from the above reaction equation, the direction of transport depends on the concentration of ATP and ADP molecules in contact with the cell membrane, as well as the substrate concentrations ($[A]_M$ and $[A]_N$). ATP molecules are abundantly produced in the cell; therefore, normally the intracellular (N side) concentration of ATP is high, which results in a positive transport flux and allows the pump to pump A out of the cell (from N to M). This is advantageous when the pump is used to exclude A from the cell. If the concentration of A_M outside the cell is very high, the pump will work in the opposite direction, and A molecules will move from outside (M) to the inside (N) of the cell while contributing to ATP production [49].

For the primary active transport mechanism, the carrier can be present in three states: the empty unloaded carrier (E), the carrier-solute complex (EA), and the carrier-solute-phosphate bound complex (EAP). Among these three states, only the unloaded carrier (E) and the phosphorylated carrier-solute complex (EAP) can cross the membrane. Upon applying symmetric assumption for the translocation rate constants of the loaded and unloaded carriers ($g_{EAP} = g_{EAP}^M = g_{EAP}^N$, $g_E = g_E^M = g_E^N$, and $g_{EAP} = g_E = g$) and the symmetric dissociation constants between carrier and substance on both sides of the membrane ($K_A = K_A^M = K_A^N$), the net flux driven across the

membrane ($J_{A,pump} = J_{A,pump}^{N,M} - J_{A,pump}^{M,N}$) is obtained from the expression [49]:

$$J_{A,pump} = [E]_t g\left(\frac{K_A\left(K_{EAP}^M[A]_M - K_{EAP}^N[A]_N\right)}{(K_{EAP}^M + K_{EAP}^N + 2K_{EAP}^M K_{EAP}^N)[A]_M[A]_N}\right.$$
$$\left.\overline{+K_A(1 + 2K_{EAP}^M)[A]_M + K_A(1 + 2K_{EAP}^N)[A]_N + 2K_A^2}\right) \tag{51}$$

Where $K_A = \frac{[A]_N[E]_N}{[EA]_N} = \frac{[A]_M[E]_M}{[EA]_M}$, $K_{EAP}^N = \frac{[EAP]_N}{[EA]_N}$, and $K_{EAP}^M = \frac{[EAP]_M}{[EA]_M}$.

Pumps simplified model:

Another method to describe the flux of ion-coupled transport across the plasma membrane by an ATPase pump is to apply the Hill model (equation 9). The Hill model of the ATPase pump is given by the expression [55, 132]:

$$J_{A,pump} = J_{A,pump}^{max}\left(\frac{[A]_N^{\eta_{pump}}}{[A]_N^{\eta_{pump}} + K_{pump}^{\eta_{pump}}}\right) \tag{52}$$

Where $J_{A,pump}^{max}$ is the maximum velocity of uptake, η_{pump} is the Hill coefficient, and K_{pump} is the $[A]_N$ concentration at which $J_{A,pump}$ is half $J_{A,pump}^{max}$. When $\eta_{pump} = 1$ this single-subtrate transport model becomes similar to the Michaelis-Menten equation, and can be written as:

$$J_{A,pump} = J_{A,pump}^{max}\left(\frac{[A]_N}{[A]_N + K_{m,pump}}\right) \tag{53}$$

The primary active transport mechanism can also transport more than one substrate. Assuming that the ATPase pump actively transports a molecules of A from the M side of the membrane to its N side and simultaneously transports b molecules of B in the opposite direction (from N to M) with the corresponding ratio $aA : bB$, and further assuming the binding of each of the components to the carrier is an independent process, the overall transport reaction mechanism can be represented as

$$ATP + aA_M + bB_N \rightleftharpoons ADP + Pi + aA_N + bB_M$$
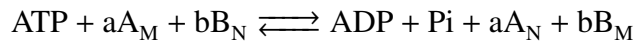
and the associated net fluxes of solutes A and B transported across the pump can be obtained using equations 54a and 54b, respectively, where the minus sign takes into account the direction

of the flux of B [133].

$$J_{A,pump} = J_{A,pump}^{max}\Big[\frac{[A]_N}{[A]_N + K_A^N}\Big]^a\Big[\frac{[B]_M}{[B]_M + K_B^M}\Big]^b \tag{54a}$$

$$J_{B,pump} = \frac{-b}{a}J_{A,pump}^{M,N} \tag{54b}$$

In equation 54a, $J_{A,pump}^{max}$ is the maximum A efflux, K_A^M, and K_B^N are the apparent dissociation constants of the complexes created at the M or N sides of the membrane, respectively.

*5.2.3. Symport transport mechanism (**J**_{Symporter}):*
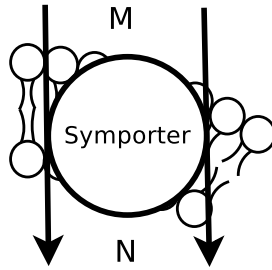
Figure 10: Symporter Transport Mechanism

Symporters are capable of co-transporting two or more solutes against the concentration gradient of one solute or group of solutes. This section includes several kinetic models of symporters, namely, *symporter slippage*, *symporter two substrates-ordered binding model*, *symporter three substrates-ordered binding model*, *symporter competitor-ordered binding model*, and the *symporter simplified model*. In the development of these models, it is assumed that the binding and unbinding of the solvent with the carrier on the two surfaces of the membrane is rapid relative to the translocation step (rapid equilibrium assumption), and that the turnover rate of the carrier-solute complex can be obtained by invoking the quasi-steady-state assumption.

Symporter Slippage:

Figure 11 depicts a possible model for a symporter with a random binding order and partial slippage during each transport cycle. In this symport system, the carrier, E, can be oriented toward the M surface of the membrane, where either substrate A or B may bind to it to form the complex EA_M or EB_M, respectively. Next, these complexes may undergo another association reaction to form the fully loaded carrier-solute complex (EAB_M) or they may face the N side of the membrane through

37

a translocation step (EA_N or EB_N). In this configuration, it is assumed that there are no restrictions on the order of binding, and carrier can cross the membrane in all states, i.e., in the empty (E), partially loaded (EA, EB), and fully loaded carrier (EAB) states, with no sequential translocation order. Turner derived the transport equation of fluxes via this transport mechanism in 1982 and Stein reproduced the kinetic scheme in 2012 [131]. Using the Turner model, the turnover rate of an individual symporter is obtained by invoking the quasi-steady-state assumption. Additionally, the binding reactions are assumed to occur much faster than the translocation steps, so that the concentration of the bound carrier can be determined using the dissociation constants (K_A, K_B, and K_{BA}). Furthermore, distinct solute dissociation constants for each step are considered, and the translocation rate constants (g_E, g_{EA}, g_{EB}, and g_{EAB}) are not necessarily equal. The rate of the net outward transport fluxes for A and B can be obtained using equations 55a and 55b, respectively [131]. In these equations, the parameters α, β, and R are related to the carrier translocation rate constants and the dissociation constants, and are expressed in terms of experimentally measurable parameters at the bottom of Figure 11.
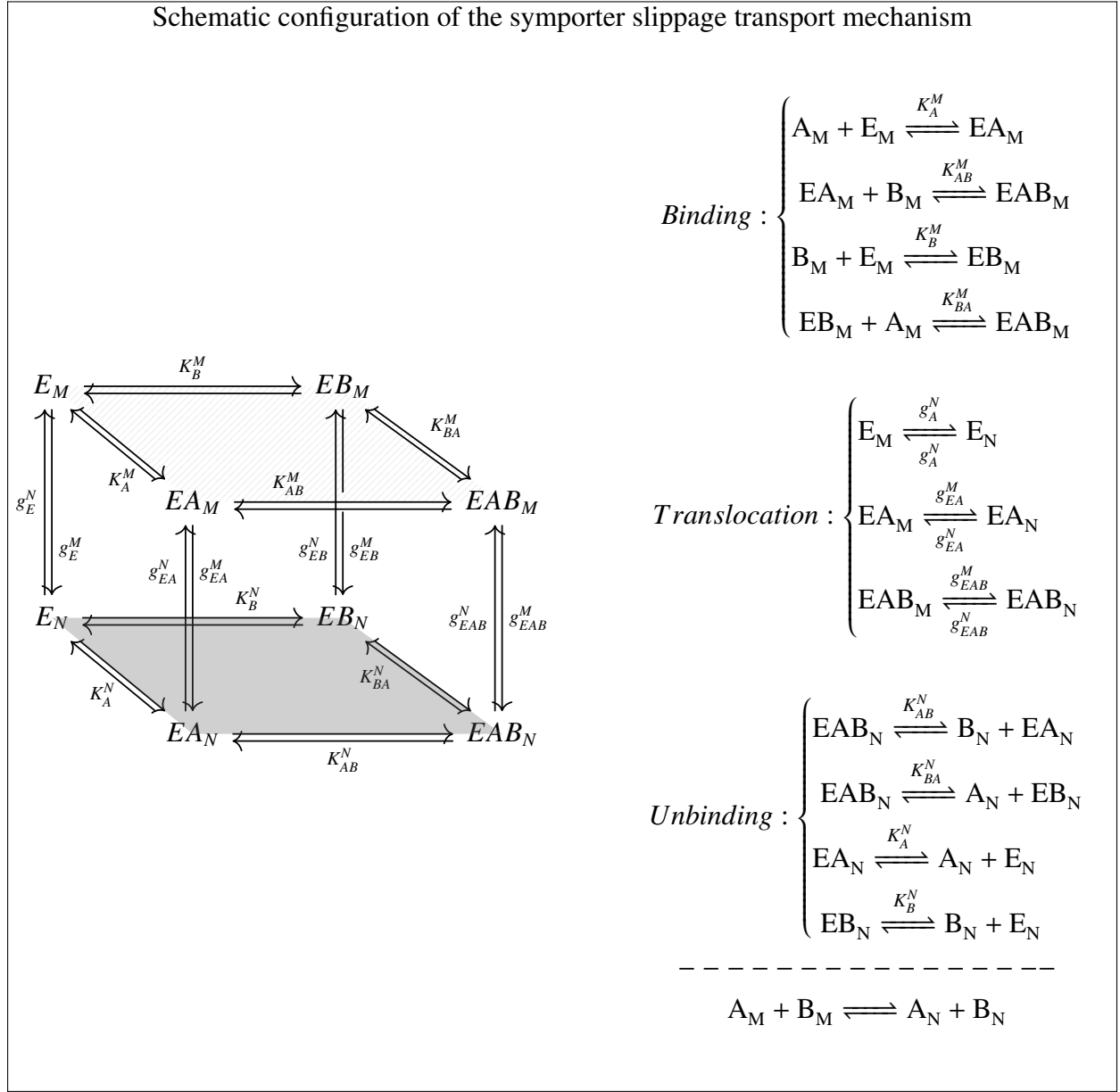
38

Figure 11: A schematic configuration of the symport slippage transport mechanism and the regarding net transport flux. Dissociation constants (K_A^M, K_{BA}^M, K_B^M) and the translocation rate constants (g_E^M, g_{EA}^M, g_{EB}^M, g_{EAB}^M) are depicted in the reaction cycle in the left panel. $[E]_t$ is the total number of transporter per unit area of the membrane. In this model empty carrier and the partially loaded carrier can slipp across the membrane. The flux equation is transformed to the general form of the resistance from Stein model [131] (part 1/2 continued on the next page).

$$J^{M,N(net)}_{A,symporter} =$$

$$[E]_t \left(\frac{(g^M_{EA}\alpha^M + g^M_{EAB}\alpha'^M\beta^M)(g^N_E + g^N_{EB}\beta^N) - (g^N_{EA}\alpha^N + g^N_{EAB}\alpha'^N\beta^N)(g^M_E + g^M_{EB}\beta^M)}{R_M R_{NN} + R_N R_{MM}} \right)$$ (55a)

$$J^{M,N(net)}_{B,symporter} =$$

$$[E]_t \left(\frac{(g^M_{EB}\beta^M + g^M_{EAB}\alpha'^M\beta^M)(g^N_E + g^N_{EA}\alpha^N) - (g^N_{EB}\beta^N + g^N_{EAB}\alpha'^N\beta^N)(g^M_E + g^M_{EA}\alpha^M)}{R_M R_{NN} + R_N R_{MM}} \right)$$ (55b)

Where

$$[E]_t = [E]_M + [EB]_M + [EA]_M + [EAB]_M + [EAB]_N + [EA]_N + [EB]_N + [E]_N$$

$$\alpha^M = \frac{[A]_M}{K^M_A}, \; \alpha'^M = \frac{[A]_M}{K^M_{BA}}, \beta^M = \frac{[B]_M}{K^M_B} \qquad \alpha^N = \frac{[A]_N}{K^N_A}, \; \alpha'^N = \frac{[A]_N}{K^N_{BA}}, \beta^N = \frac{[B]_N}{K^N_B}$$

$$R_M = (1 + \alpha^M + \beta^M + \alpha'^M\beta^M) \qquad R_N = (1 + \alpha^N + \beta^N + \alpha'^N\beta^N)$$

$$R_{MM} = g^M_E + g^M_{EA}\alpha^M + g^M_{EB}\beta^M + g^M_{EAB}\alpha'^M\beta^M \qquad R_{NN} = g^N_E + g^N_{EA}\alpha^N + g^N_{EB}\beta^N + g^N_{EAB}\alpha'^N\beta^N$$

Figure 11: A schematic configuration of the symport slippage transport mechanism and the regarding net flux transport equation. Dissociation constants (K^M_A, K^M_{BA}, K^M_B) and the translocation rate constants (g^M_E, g^M_{EA}, g^M_{EB}, g^M_{EAB}) are depicted in the reaction cycle in the left panel. $[E]_t$ is the total number of transporter per unit area of the membrane. In this model empty carrier and the partially loaded carrier can slipp across the membrane. The flux equation is transformed to the general form of the resistance from Stein model [131] (part 2/2 continued from previous page).

Two-substrate symporter ordered binding models:

Kinetic schemes for sequential binding (ordered binding) cotransport mechanisms involving two solutes are depicted in Figures 12 and 13. When A binds first, the symport transport mechanism shown in Figure 12 applies, and the corresponding net flux of A and B through the symporter can be expressed using equations 56b and 56c, respectively. Similarly, the mechanism for the case in which B binds first is illustrated in Figure 13, and the corresponding net outward flux of A and B can be obtained using equations 57b and 57c, respectively. In these equations, $J^{M,N(net)}_{symporter}$ is the steady-state turnover rate of the symporter (expressed in equations 56a and 57a, accordingly), and the parameters α, β, and R are related to the carrier translocation rate constants and the dissociation constants, which are expressed in terms of experimentally measurable parameters at the bottom of the Figures 12 and 13, accordingly. These models were developed and parameterized by Stein (2012) [131]. In these models, it is assumed that the partially loaded carriers (*EA* and *EB*) cannot

489 translocate at either side of the membrane, and only the fully loaded carrier (*EAB*) is able to cross

490 the membrane.

Schematic configuration of the two-substrate symporter ordered binding transport mechanism, where A binds first

$$\begin{cases} A_M + E_M \xrightleftharpoons{K_A^M} EA_M \mid EA_M + B_M \xrightleftharpoons{K_{AB}^M} EAB_M \end{cases}$$

$$E_M \xrightleftharpoons{K_A^M} EA_M \xrightleftharpoons{K_{AB}^M} EAB_M$$

$$\begin{cases} E_M \underset{g_E^N}{\overset{g_E^M}{\rightleftharpoons}} E_N \\ EAB_M \underset{g_{EAB}^N}{\overset{g_{EAB}^M}{\rightleftharpoons}} EAB_N \end{cases}$$

$$g_E^N \Big\| g_E^M \qquad g_{EAB}^N \Big\| g_{EAB}^M$$

$$E_N \xrightleftharpoons{K_A^N} EA_N \xrightleftharpoons{K_{AB}^N} EAB_N$$

$$\begin{cases} EAB_N \xrightleftharpoons{K_{AB}^N} EA_N + B_N \mid EA_N \xrightleftharpoons{K_A^N} A_N + E_N \end{cases}$$

$$- - - - - - - - - - - - - - - - - - - -$$

$$A_M + B_M \rightleftharpoons A_N + B_N$$

Net Transport Flux from M to N

$$J_{symporter}^{M,N(net)} = [E]_t \frac{(g_{EAB}^M \alpha^M \beta^M)g_E^N - (g_{EAB}^N \alpha^N \beta^N)g_E^M}{R_M R_{NN} + R_N R_{MM}} \tag{56a}$$

$$J_{A,symporter}^{M,N(net)} = J_{symporter}^{M,N(net)} \tag{56b}$$

$$J_{B,symporter}^{M,N(net)} = J_{symporter}^{M,N(net)} \tag{56c}$$

where
$$[E]_t = [E]_M + [EA]_M + [EAB]_M + [EAB]_N + [EA]_N + [E]_N$$

$$\alpha^M = \frac{[A]_M}{K_A^M}, \qquad \beta^M = \frac{[B]_M}{K_{AB}^M} \qquad\qquad \alpha^N = \frac{[A]_N}{K_A^N}, \qquad \beta^N = \frac{[B]_N}{K_{AB}^N}$$
$$R_M = (1 + \alpha^M + \alpha^M \beta^M) \qquad\qquad R_N = (1 + \alpha^N + \alpha^N \beta^N)$$
$$R_{MM} = (g_E^M + g_{EAB}^M \alpha^M \beta^M) \qquad\qquad R_{NN} = (g_E^N + g_{EAB}^N \alpha^N \beta^N)$$

Figure 12: A schematic configuration and the regarding net flux transport equation of the symporter ordered binding with no slippage, for transport of two solutes where A binds first. Dissociation constants (K_A and K_{AB} terms) and the translocation rate constants (g_E and g_{EAB} terms) are depicted in the reaction cycle in the left panel. $[E]_t$ is the total number of transporter per unit area of the membrane. The flux equation is transformed to the general form of the resistance from Stein model [131].

Schematic configuration of the two-substrate symporter ordered binding transport mechanism, where B binds first

$$B_M + E_M \xrightleftharpoons{K_B^M} EB_M \mid EB_M + A_M \xrightleftharpoons{K_{BA}^M} EBA_M$$

$$E_M \xrightleftharpoons{K_B^M} EB_M \xrightleftharpoons{K_{BA}^M} EAB_M$$

$$E_M \underset{g_E^N}{\overset{g_E^M}{\rightleftharpoons}} E_N$$

$$EBA_M \underset{g_{EBA}^N}{\overset{g_{EBA}^M}{\rightleftharpoons}} EBA_N$$

$$E_N \xrightleftharpoons{K_B^N} EB_N \xrightleftharpoons{K_{BA}^N} EAB_N$$

$$EBA_N \xrightleftharpoons{K_{BA}^N} EB_N + A_N \mid EB_N \xrightleftharpoons{K_B^N} B_N + E_N$$

$$B_M + A_M \rightleftharpoons A_N + B_N$$

(with vertical translocation rates g_E^N, g_E^M and g_{EAB}^N, g_{EAB}^M)

Net Transport Flux from M to N

$$J_{symporter}^{M,N(net)} = [E]_t \frac{(g_{EAB}^M \alpha'^M \beta^M) g_E^N - (g_{EAB}^N \alpha'^N \beta^N) g_E^M}{R_M R_{NN} + R_N R_{MM}} \tag{57a}$$

$$J_{A,symporter}^{M,N(net)} = J_{symporter}^{M,N(net)} \tag{57b}$$

$$J_{B,symporter}^{M,N(net)} = J_{symporter}^{M,N(net)} \tag{57c}$$

where
$$[E]_t = [E]_M + [EB]_M + [EAB]_M + [EAB]_N + [EB]_N + [E]_N$$

$$\alpha'^M = \frac{[A]_M}{K_{BA}^M}, \qquad \beta^M = \frac{[B]_M}{K_B^M}$$
$$R_M = (1 + \beta^M + \alpha'^M \beta^M)$$
$$R_{MM} = g_E^M + g_{EAB}^M \alpha'^M \beta^M$$

$$\alpha'^N = \frac{[A]_N}{K_{BA}^N}, \qquad \beta^N = \frac{[B]_N}{K_B^N}$$
$$R_N = (1 + \beta^N + \alpha'^N \beta^N)$$
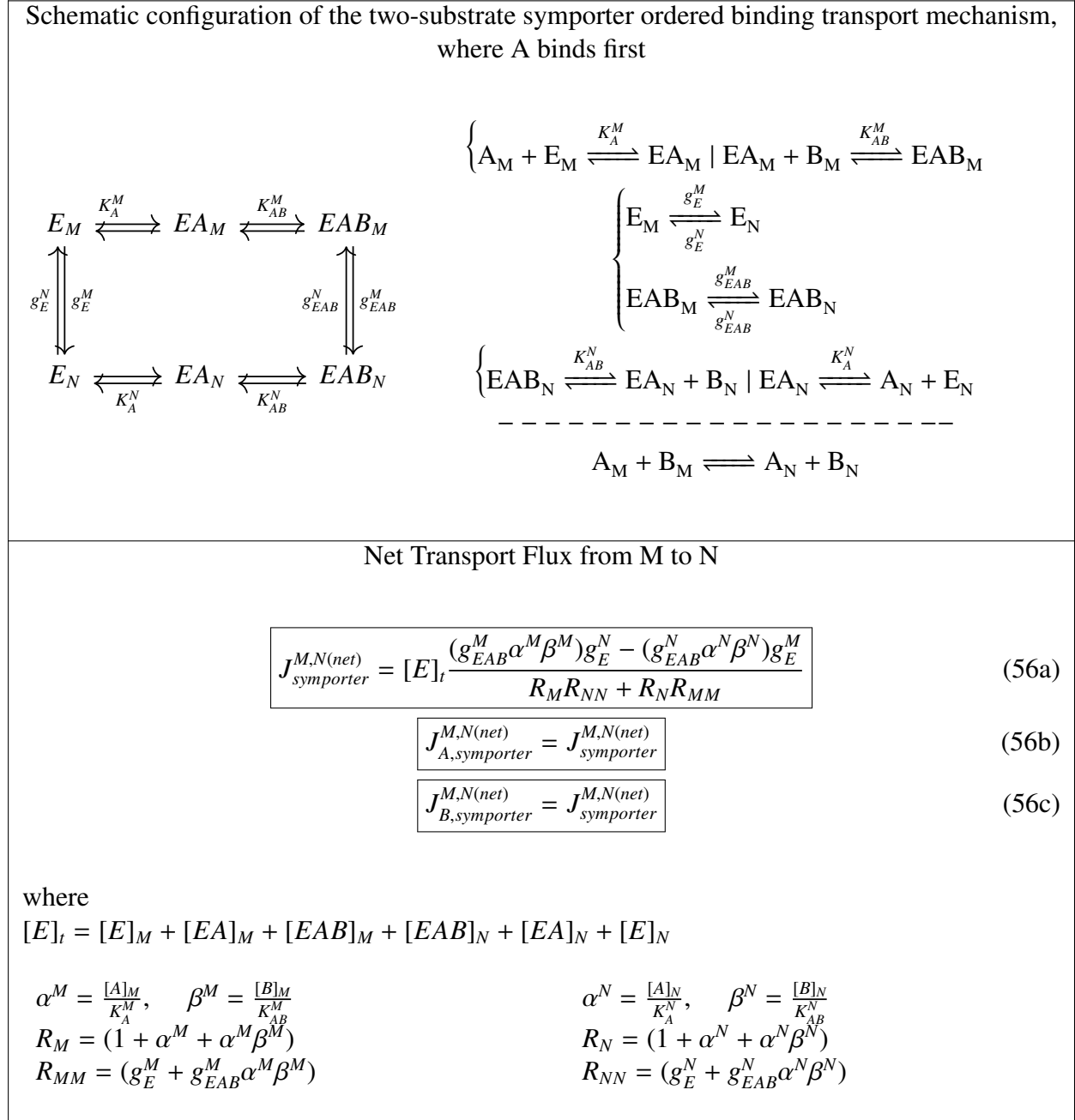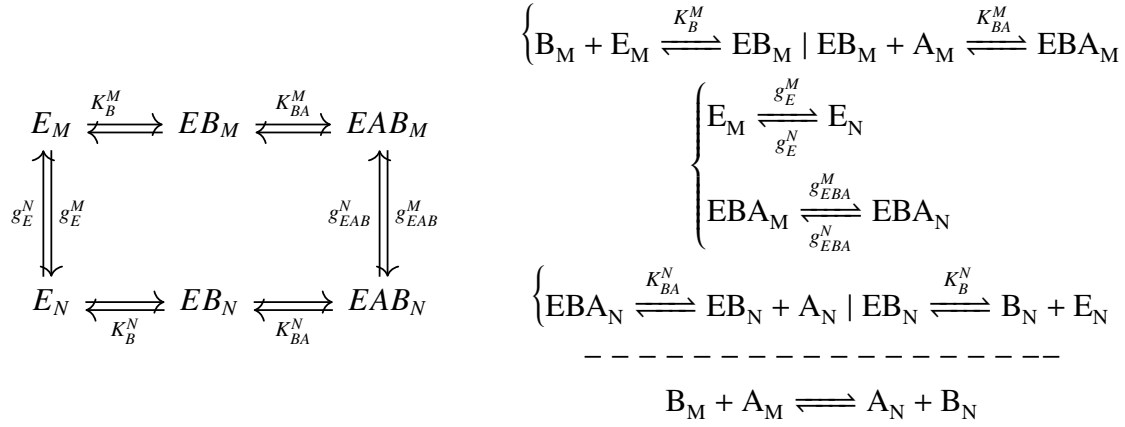$$R_{NN} = g_E^N + g_{EAB}^N \alpha'^N \beta^N$$

Figure 13: A schematic configuration and the regarding net flux transport equation of the symporter mechanism with no slippage, for transport of two solutes where binding happens in order and B binds first. Dissociation constants (K_{BA} and K_B terms) and the translocation rate constants (g_E and g_{EAB} terms) are depicted in the reaction cycle in the right panel. $[E]_t$ is the total number of transporter per unit area of the membrane. The flux equation is transformed to the general resistance form from Stein model [131].

Three-substrate symporter ordered binding model:

Figure 14 shows a kinetic scheme for a carrier, E, that is capable of transporting molecules of A,

B, and C in a ratio of $2A : B : C$ and exhibits a sequential binding order. In the first step, the carrier faces the M side of the membrane and binds to a molecule of A. After the complex EA_M is formed, a molecule of B binds to EA_M to form the EAB_M complex, followed by the binding of a second molecule of A to form complex $EABA_M$. Finally, a molecule of C binds to the transporter to give the fully loaded carrier complex $EABAC_M$. In this model, the carriers can translocate across the membrane in all states (i.e., in the empty, partially loaded, and fully loaded states), and the unbinding reactions occur in the reverse order of binding. This is referred to as a "first on last off" binding order, since the molecule which binds first (e.g., A) on one side of the membrane is the last to unbind from the other side of the membrane. A transport model for this mechanism was first developed by Delpire (2011). In this work, the kinetic parameterization method of Stein (2012) is followed, and the net outward fluxes of A, B, and C transported through the cotransporter are represented by equations 58a, 58b, and 58c, respectively.

Schematic configuration of the ABAC symporter transport mechanism,
where the order of binding is A, B, second A, and C
and the unbinding reactions occur in the reverse order of binding

$$E_M \xrightleftharpoons{K_A^M} EA_M \xrightleftharpoons{K_{AB}^M} EAB_M \xrightleftharpoons{K_{ABA}^M} EABA_M \xrightleftharpoons{K_{ABAC}^M} EABAC_M$$

$$g_E^N \Big\| g_E^M \quad g_{EA}^N \Big\| g_{EA}^M \quad g_{EAB}^N \Big\| g_{EAB}^M \quad g_{EABA}^N \Big\| g_{EABA}^M \quad g_{EABAC}^N \Big\| g_{EABAC}^M$$

$$E_N \xrightleftharpoons{K_A^N} EA_N \xrightleftharpoons{K_{AB}^N} EAB_N \xrightleftharpoons{K_{ABA}^N} EABA_N \xrightleftharpoons{K_{ABAC}^N} EABAC_N$$

$$\begin{cases} A_M + E_M \xrightleftharpoons{K_A^M} EA_M \mid EA_M + B_M \xrightleftharpoons{K_{AB}^M} EAB_M \\ EAB_M + A_M \xrightleftharpoons{K_{ABA}^M} EABA_M \mid EABA_M + C_M \xrightleftharpoons{K_{ABAC}^M} EABAC_M \end{cases}$$

$$\begin{cases} EABAC_M \xrightleftharpoons[g_{EABAC}^N]{g_{EABAC}^M} EABAC_N \\[2mm] EABA_M \xrightleftharpoons[g_{EABA}^N]{g_{EABA}^M} EABA_N \\[2mm] EAB_M \xrightleftharpoons[g_{EAB}^N]{g_{EAB}^M} EAB_N \\[2mm] EA_M \xrightleftharpoons[g_{EA}^N]{g_{EA}^M} EA_N \\[2mm] E_M \xrightleftharpoons[g_E^N]{g_E^M} E_N \end{cases}$$

$$\begin{cases} EABAC_N \xrightleftharpoons{K_{ABAC}^N} EABA_N + C_N \mid EABA_N \xrightleftharpoons{K_{ABA}^N} EAB_N + A_N \\ EAB_N \xrightleftharpoons{K_{AB}^N} EA_N + B_N \mid EA_N \xrightleftharpoons{K_A^N} E_N + A_N \end{cases}$$

– –

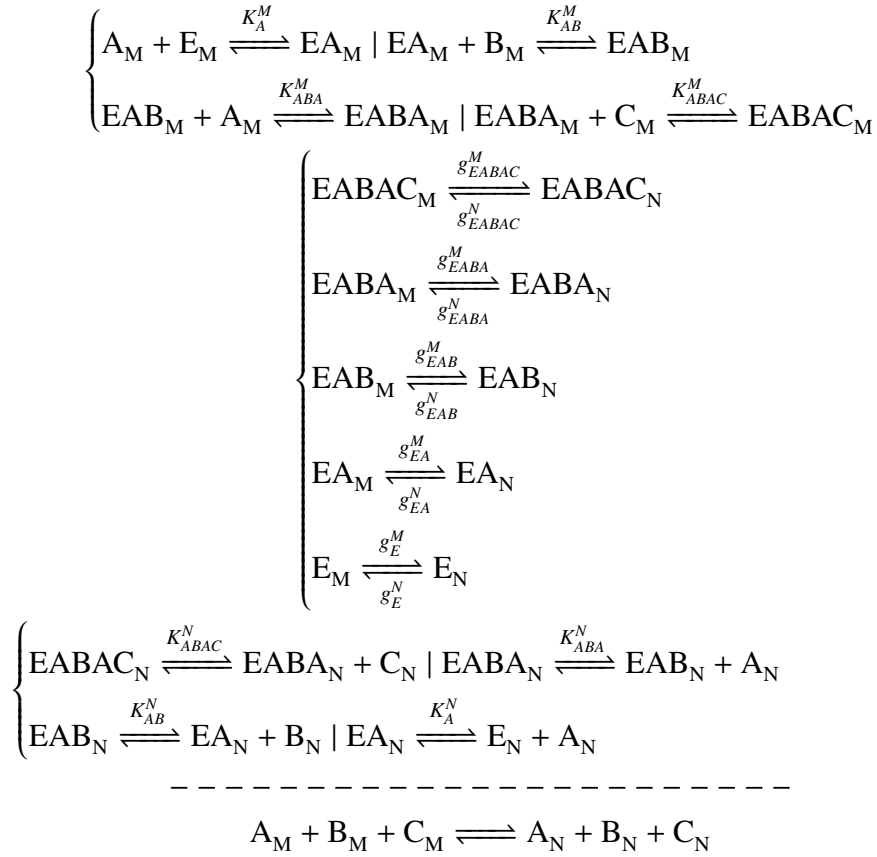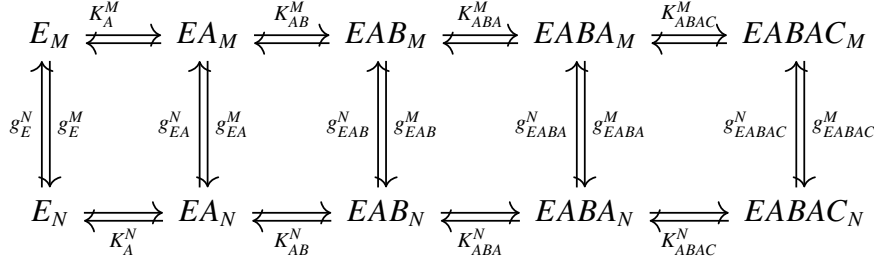$$A_M + B_M + C_M \rightleftharpoons A_N + B_N + C_N$$

Figure 14: A schematic configuration of the ABAC symporter mechanism transporting of three solutes and the regarding net flux transport equation. In this configuration, the carrier exists in 5 different states on each side of the membrane. Dissociation constants (K_A, K_{AB}, K_{ABA} , and K_{ABAC} terms) and the translocation rate constants (g_E, g_{EA}, g_{EAB}, g_{EABA}, and g_{EABAC} terms) are depicted in the reaction cycle in the right panel. $[E]_t$ is the total number of transporter per unit area of the membrane. Transport equations are reparametrized and transformed into the general resistance form from Delpire model [134] (part 1/2 continued on next page).

Net Transport Flux from M to N	

$$J^{M,N(net)}_{A,symporter} = [E]_t$$

$$\left(\frac{R_{NN}\left(g^M_{EA}\alpha^M + g^M_{EAB}\alpha^M\beta^M + g^M_{EABA}\alpha^M\beta^M\alpha''^M + g^M_{EABAC}\alpha^M\beta^M\alpha''^M\gamma^M\right)}{R_M R_{NN} + R_N R_{MM}} \right.$$

$$\left. - \frac{R_{MM}\left(g^N_{EA}\alpha^N + g^N_{EAB}\alpha^N\beta^N + g^N_{EABA}\alpha^N\beta^N\alpha''^N + g^N_{EABAC}\alpha^N\beta^N\alpha''^N\gamma^N\right)}{R_M R_{NN} + R_N R_{MM}} \right)$$

(58a)

$$J^{M,N(net)}_{B,symporter} = [E]_t$$

$$\left(\frac{R_{NN}\left(g^M_{EAB}\alpha^M\beta^M + g^M_{EABA}\alpha^M\beta^M\alpha''^M + g^M_{EABAC}\alpha^M\beta^M\alpha''^M\gamma^M\right)}{R_M R_{NN} + R_N R_{MM}} \right.$$

$$\left. - \frac{R_{MM}\left(g^N_{EAB}\alpha^N\beta^N + g^N_{EABA}\alpha^N\beta^N\alpha''^N + g^N_{EABAC}\alpha^N\beta^N\alpha''^N\gamma^N\right)}{R_M R_{NN} + R_N R_{MM}} \right)$$

(58b)

$$J^{M,N(net)}_{C,symporter} = [E]_t\left(\frac{R_{NN}(g^M_{EABAC}\alpha^M\beta^M\alpha''^M\gamma^M) - R_{MM}(g^N_{EABAC}\alpha^N\beta^N\alpha''^N\gamma^N)}{R_M R_{NN} + R_N R_{MM}} \right)$$

(58c)

where

$$[E]_t = [E]_M + [EA]_M + [EAB]_M + [EABA]_M + [EABAC]_M + [EABAC]_N + [EABA]_N + [EAB]_N + [EA]_N + [E]_N$$

$$\alpha^M = \frac{[A]_M}{K^M_A}, \beta^M = \frac{[B]_M}{K^M_{AB}}, \alpha''^M = \frac{[A]_M}{K^M_{ABA}}, \gamma^M = \frac{[C]_M}{K^M_{ABAC}}$$

$$\alpha^N = \frac{[A]_N}{K^N_A}, \beta^N = \frac{[B]_N}{K^N_{AB}}, \alpha''^N = \frac{[A]_N}{K^N_{ABA}}, \gamma^N = \frac{[C]_N}{K^N_{ABAC}}$$

$$R_M = 1 + \alpha^M + \alpha^M\beta^M + \alpha^M\beta^M\alpha''^M + \alpha^M\beta^M\alpha''^M\gamma^M$$

$$R_N = 1 + \alpha^N + \alpha^N\beta^N + \alpha^N\beta^N\alpha''^N + \alpha^N\beta^N\alpha''^N\gamma^N$$

$$R_{MM} = g^M_E + g^M_{EA}\alpha^M + g^M_{EAB}\alpha^M\beta^M + g^M_{EABA}\alpha^M\beta^M\alpha''^M + g^M_{EABAC}\alpha^M\beta^M\alpha''^M\gamma^M$$

$$R_{NN} = g^N_E + g^N_{EA}\alpha^N + g^N_{EAB}\alpha^N\beta^N + g^N_{EABA}\alpha^N\beta^N\alpha''^N + g^N_{EABAC}\alpha^N\beta^N\alpha''^N\gamma^N$$

Figure 14: A schematic configuration of the ABAC symporter mechanism transporting of three solutes and the regarding net flux transport equation. In this configuration, the carrier exists in 5 different states on each side of the membrane. Dissociation constants (K_A, K_{AB}, K_{ABA} , and K_{ABAC} terms) and the translocation rate constants (g_E, g_{EA}, g_{EAB}, g_{EABA}, and g_{EABAC} terms) are depicted in the reaction cycle in the right panel. $[E]_t$ is the total number of transporter per unit area of the membrane. Transport equations are reparametrized and transformed into the general resistance form from Delpire model [134] (part 2/2 continued from previous page).

Figure 15 depicts a different binding/unbinding order for multiple solutes on a carrier. In the scheme, the stoichiometric ratio of the transport reaction is $A : 2B : C$ and the order of binding is as follows: first, solute A binds to the carrier on surface M of the membrane to form the complex EA_M

then the first molecule of B binds to EA_M to form the complex EAB_M is formed. This binding is

followed by the binding of substrate C and the formation of the complex $EABC_M$ complex. In the

last binding step, the second molecule of B is bound, and the full complex ($EABCB_M$) is formed

on the M face of the membrane. In this work, the model of the kinetic-transport mechanism is

driven by applying Stein's (2012) parameterization method, and the overall transport fluxes of A,

B, and C are expressed in equations 59b, 59c, and 59d, respectively.

Schematic configuration of the ABCB symporter first on- first off transport mechanism, where order of binding is A,B,C, and second B and the order of unbinding is A, B, C, and B

$$E_M \xrightleftharpoons{K_A^M} EA_M \xrightleftharpoons{K_{AB}^M} EAB_M \xrightleftharpoons{K_{ABC}^M} EABC_M \xrightleftharpoons{K_{ABCB}^M} EABCB_M$$

$$g_E^N \,\|\, g_E^M \qquad\qquad\qquad\qquad g_{EABCB}^N \,\|\, g_{EABCB}^M$$

$$E_N \xrightleftharpoons[K_B^N]{} EB_N \xrightleftharpoons[K_{CB}^N]{} ECB_N \xrightleftharpoons[K_{BCB}^N]{} EBCB_N \xrightleftharpoons[K_{ABCB}^N]{} EABCB_N$$

$$\begin{cases} A_M + E_M \xrightleftharpoons{K_A^M} EA_M \mid EA_M + B_M \xrightleftharpoons{K_{AB}^M} EAB_M \\ EAB_M + C_M \xrightleftharpoons{K_{ABC}^M} EABC_M \mid EABC_M + B_M \xrightleftharpoons{K_{ABCB}^M} EABCB_M \end{cases}$$

$$\begin{cases} E_M \xrightleftharpoons[g_E^N]{g_E^M} E_N \\ EABCB_M \xrightleftharpoons[g_{EABCB}^N]{g_{EABCB}^M} EABCB_N \end{cases}$$

$$\begin{cases} EABCB_N \xrightleftharpoons{K_{ABCB}^N} EBCB_N + A_N \mid EBCB_N \xrightleftharpoons{K_{BCB}^N} ECB_N + B_N \\ ECB_N \xrightleftharpoons{K_{CB}^N} EB_N + C_N \mid EB_N \xrightleftharpoons{K_B^N} E_N + B_N \end{cases}$$

$$- -$$

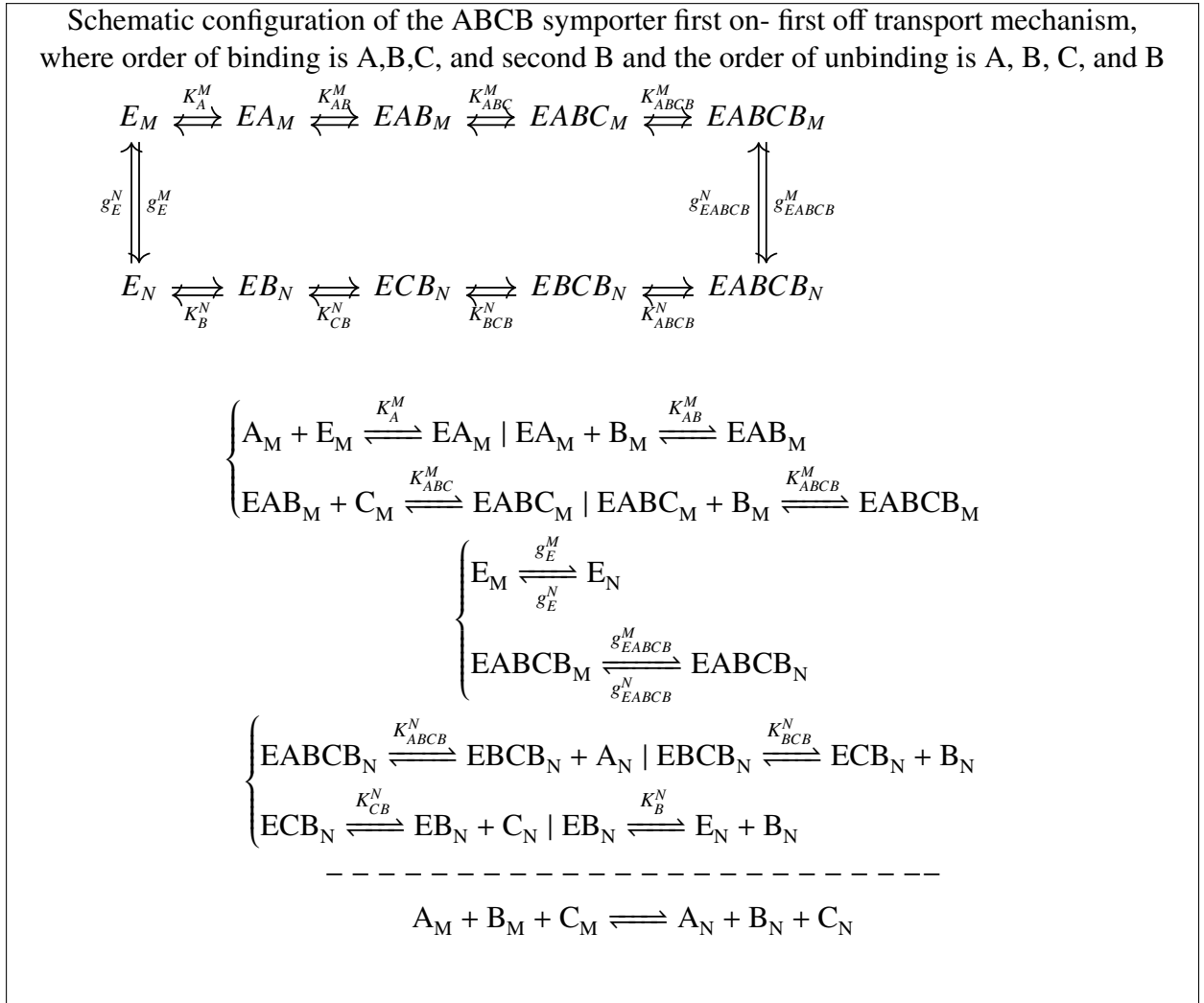$$A_M + B_M + C_M \rightleftharpoons A_N + B_N + C_N$$

Figure 15: A schematic configuration of the symporter mechanism transporting three solutes (ABCB), and the corresponding net transported flux equation. In this configuration, the carrier exists in 5 different states on each side of the membrane. Dissociation constants (K_A, K_{AB}, K_{ABC}, K_{ABCB}, K_{BCB}, K_{CB}, and K_B terms), and the translocation rate constants (g_E and g_{EABCB} terms) are depicted in the reaction cycle in the right panel. $[E]_t$ is the total number of transporter per unit area of the membrane (part 1/2 continued on next page).

$$J_{symporter}^{M,N(net)} = [E]_t \left(\frac{\left(g_{EABCB}^M \alpha^M \beta^M \gamma^M \beta''^M \right) g_E^N - \left(g_{EABCB}^N \alpha^N \beta^N \gamma^N \beta''^N \right) g_E^M}{R_M R_{NN} + R_N R_{MM}} \right) \qquad (59a)$$

$$J_{A,symporter}^{M,N(net)} = J_{symporter}^{M,N(net)} \qquad (59b)$$

$$J_{B,symporter}^{M,N(net)} = 2 J_{symporter}^{M,N(net)} \qquad (59c)$$

$$J_{C,symporter}^{M,N(net)} = J_{symporter}^{M,N(net)} \qquad (59d)$$

where
$$[E]_t = [E]_M + [EA]_M + [EAB]_M + [EABC]_M + [EABCB]_M + [EABCB]_N + [EABC]_N + [EAB]_N + [EA]_N + [E]_N$$

$$\alpha^M = \frac{[A]_M}{K_A^M}, \quad \beta^M = \frac{[B]_M}{K_{AB}^M}, \qquad\qquad \gamma^M = \frac{[C]_M}{K_{ABC}^M}, \quad \beta''^M = \frac{[B]_M}{K_{ABCB}^M},$$
$$\alpha^N = \frac{[A]_N}{K_{ABCB}^N}, \quad \beta^N = \frac{[B]_N}{K_{BCB}^N} \qquad \gamma^N = \frac{[C]_N}{K_{CB}^N}, \quad \beta''^N = \frac{[B]_N}{K_B^N}$$

$$R_M = 1 + \alpha^M + \alpha^M \beta^M + \alpha^M \beta^M \gamma^M + \alpha^M \beta^M \gamma^M \beta''^M$$
$$R_N = 1 + \beta''^N + \gamma^N \beta''^N + \beta^N \gamma^N \beta''^N + \alpha^N \beta^N \gamma^N \beta''^N$$
$$R_{MM} = g_E^M + g_{EABCB}^M \alpha^M \beta^M \gamma^M \beta''^M$$
$$R_{NN} = g_E^N + g_{EABCB}^N \alpha^N \beta^N \gamma^N \beta''^N$$

Figure 15: A schematic configuration of the symporter mechanism transporting three solutes (ABCB), and the corresponding net transported flux equation. In this configuration, the carrier (cotransporter) exists in 5 different states on each side of the membrane. Dissociation constants (K_A, K_{AB}, K_{ABC}, K_{ABCB}, K_{BCB}, K_{CB}, and K_B terms), and the translocation rate constants (g_E and g_{EABCB} terms) are depicted in the reaction cycle in the right panel. $[E]_t$ is the total number of transporter per unit area of the membrane (part 2/ 2 continued from last page).

Competitive symporter ordered binding model:

Figure 16 shows a competitive symport transport mechanism involving substrates *A*, *B*, and *C*, in which *C* competes with *B* for the same binding sites on the carrier. In the first step, a molecule of *A* binds to the empty carrier (*E*), followed by the binding of a *B* or *C* molecule to form the complex EAB or *EAC*, respectively. Next, the formed complexes cross the membrane (EAC_N or EAB_N), where they undergo dissociation reactions in which A unbinds last from both complexes. In this model, it is assumed that the carrier can exist in four different states at each side of the membrane, that only the fully loaded (*EAB* and *EAC*) and empty carriers (E) can cross the membrane. The net

$_{522}$ outward fluxes of *B*, *C*, and *A* can be obtained through equations 60a, 60b, and 60c, respectively.

$_{523}$ This model can also be applied to the symport transport mechanism of three substrates in a ratio

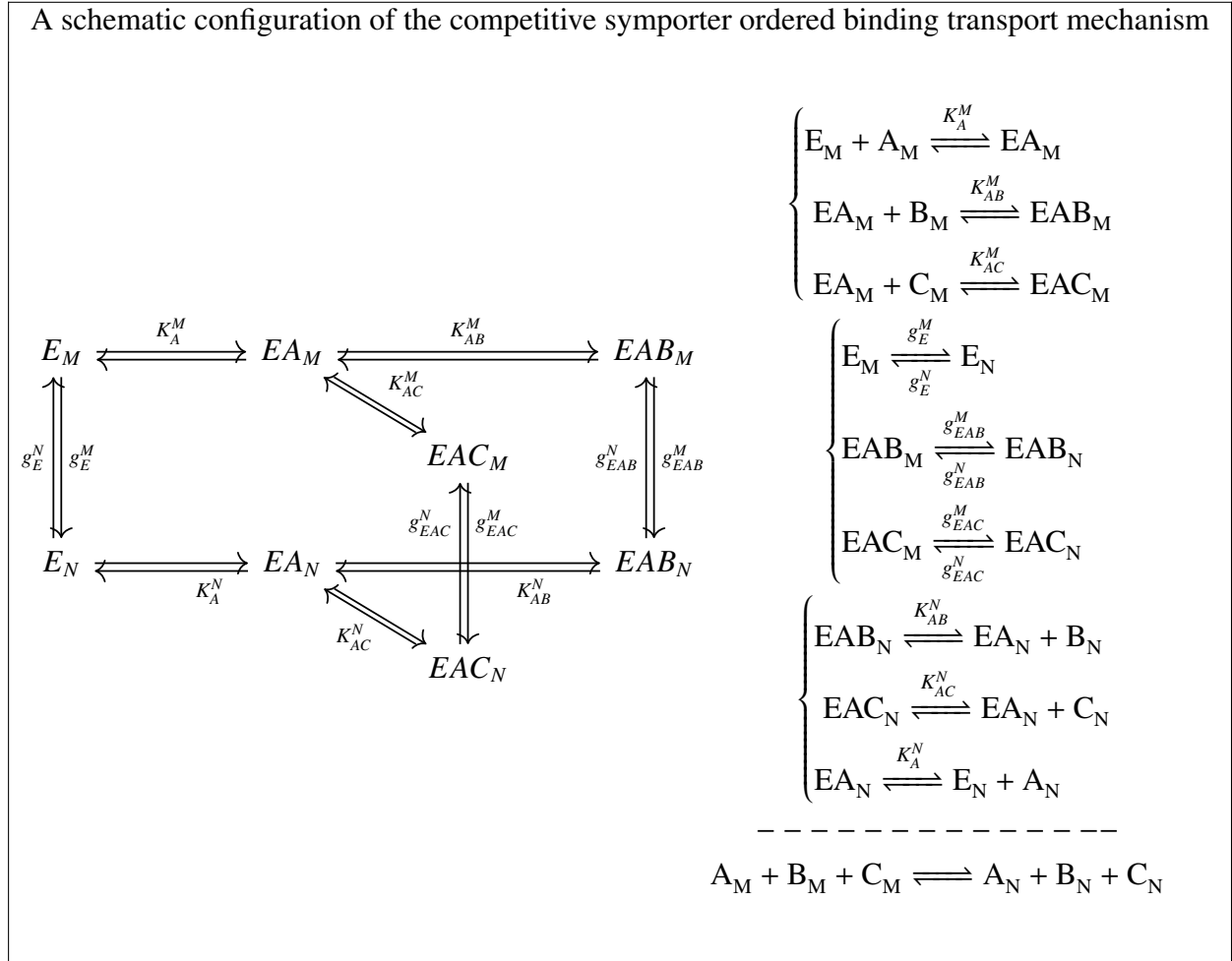$_{524}$ of $A : B : C$ [100].

Figure 16: A schematic configuration of the competitive symporter ordered binding transport mechanism of two solutes and the regarding net flux transport equation. In this configuration, the carrier exists in four different states on each surface of the membrane. Transport equations are reparametrized and transformed into the general resistance form from Layton model [100]. Dissociation constants (K_A, K_{AB}, K_{AC} terms), and the translocation rate constants (g_E, g_{EAC}, and g_{EAB} terms) are depicted in the reaction cycle in the right panel. Subscripts M and N, denote the M and N sides of the cell membrane (part 1/2 continued on next page).

Net Transport Flux from M to N	
$$J_{B,symporter}^{M,N(net)} = [E]_t \frac{\left(g_{EAB}^M \alpha^M \beta^M\right) R_{NN} - \left(g_{EAB}^N \alpha^N \beta^N\right) R_{MM}}{R_M R_{NN} + R_N R_{MM}}$$	(60a)
$$J_{C,symporter}^{M,N(net)} = [E]_t \frac{\left(g_{EAC}^M \alpha^M \gamma^M\right) R_{NN} - \left(g_{EAC}^N \alpha^N \gamma^N\right) R_{MM}}{R_M R_{NN} + R_N R_{MM}}$$	(60b)
$$J_{A,symporter}^{M,N(net)} = [E]_t \frac{\left(g_{EAB}^M \alpha^M \beta^M + g_{EAC}^M \alpha^M \gamma^M\right) R_{NN} - \left(g_{EAB}^N \alpha^N \beta^N + g_{EAC}^N \alpha^N \gamma^N\right) R_{MM}}{R_M R_{NN} + R_N R_{MM}}$$	(60c)

where
$$[E]_t = [E]_M + [EA]_M + [EAB]_M + [EAC]_M + [EAC]_N + [EAB]_N + [EA]_N + [E]_N$$

$\alpha^M = \frac{[A]_M}{K_A^M}, \beta^M = \frac{[B]_M}{K_{AB}^M}, \gamma^M = \frac{[C]_M}{K_{AC}^M}$ $\qquad$ $\alpha^N = \frac{[A]_N}{K_A^N}, \beta^N = \frac{[B]_N}{K_{AB}^N}, \gamma^N = \frac{[C]_N}{K_{AC}^N}$

$R_M = 1 + \alpha^M + \alpha^M \beta^M + \alpha^M \gamma^M$ $\qquad$ $R_N = 1 + \alpha^N + \alpha^N \beta^N + \alpha^N \gamma^N$
$R_{MM} = g_E^M + g_{EAB}^M \alpha^M \beta^M + g_{EAC}^M \alpha^M \gamma^M$ $\qquad$ $R_{NN} = g_E^N + g_{EAB}^N \alpha^N \beta^N + g_{EAC}^N \alpha^N \gamma^N$

Figure 16: A schematic configuration of the competitive symporter ordered binding transport mechanism of two solutes and the regarding net flux transport equation. In this configuration, the carrier exists in four different states on each side of the membrane. Transport equations are reparametrized and transformed into the general resistance form from Layton model [100]. Dissociation constants (K_A, K_{AB}, K_{AC} terms), and the translocation rate constants (g_E, g_{EAC}, and g_{EAB} terms) are depicted in the reaction cycle in the right panel. Subscripts M and N, denote the M and N sides of the cell membrane. $[E]_t$ is the total number of transporter per unit area of the membrane (part 2/2 continued from previous page).

Symporter simplified model:

To conclude the section on symporters, a commonly used reduced symporter carrier model is presented. In this model, the rapid-equilibrium assumption, quasi-steady-state assumption, and symmetric carrier assumption ($K_A^M = K_A^N = K_A$, $K_B^M = K_B^N = K_B$, $K_C^M = K_C^N = K_C$) are invoked. Furthermore, it is assumed the binding and unbinding steps do not follow a particular sequential order. Under these assumptions, for the general case of a symporter transporting three solutes in the ratio of $aA : bB : cC$, the net outward symporter turnover rate is given by equation 61a and the corresponding solute fluxes of A, B, and C are given by equations 61b, 61c, and 61d, respectively.

A general simplified model of symporter with three substrates
$aA_M + bB_M + cC_M \rightleftharpoons aA_N + bB_N + cC_N$

Net Transport Flux from M to N	
$J_{symporter}^{M,N(net)} = P_{symporter} \dfrac{[A]_M^a [B]_M^b [C]_M^c - [A]_N^a [B]_N^b [C]_N^c}{\left[\alpha^N + 1\right]^a \left[\beta^N + 1\right]^b \left[\gamma^N + 1\right]^c}$	(61a)
$J_{A,symporter}^{M,N(net)} = a J_{symporter}^{M,N(net)}$	(61b)
$J_{B,symporter}^{M,N(net)} = b J_{symporter}^{M,N(net)}$	(61c)
$J_{C,symporter}^{M,N(net)} = c J_{symporter}^{M,N}$	(61d)

where $P_{symporter} = [E]_t g_{symporter}$ is the membrane permeability to the symporter and its value can be found experimentally [135].

The thermodynamic parameters are defined as:

$$\alpha^M = \frac{[A]_M}{K_A}, \quad \beta^M = \frac{[B]_M}{K_B}, \quad \gamma^M = \frac{[C]_M}{K_C} \qquad\qquad \alpha^N = \frac{[A]_N}{K_A}, \quad \beta^N = \frac{[B]_N}{K_B}, \quad \gamma^N = \frac{[C]_N}{K_C}$$

Figure 17: Symporter simplified model. The following assumptions are used: (1) the rapid binding and unbinding assumption, (2) the quasi-steady-state assumption, (3) symmetric carrier assumption (similarity for all rate constants), (4) symporter has a single site which bound the transported solute, (5) the transported solute competed for the same binding sites, and (6) finally, the empty symporter does not cross the membrane (there is no slippage of empty carrier).

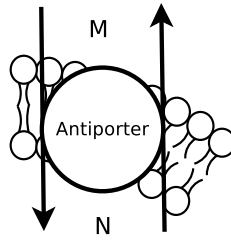### 5.2.4. Antiporter transport mechanism ($J_{antiporter}$):

Figure 18: Antiporter Transport Mechanism

Antiporters, which are also known as exchangers, are modeled very similarly to symporters.This section covers several commonly used antiporter models, namely, the *eight-state antiporter ordered binding* model, *six-state antiporter ordered binding* model, *competitive antiporter ordered-*

50

binding model, and *simplified antiporter* model.

Eight-state antiporter ordered binding model:

Figure 19 shows a scheme of an antiporter transport mechanism in which the substrate *A* moves from M to N while *B* is simultaneously transported in the opposite direction. This model is known as the "eight-state" mechanism, as the carrier can exist in eight forms at the two sides of the membrane (E_M, EA_M, EB_M, EAB_M, E_N, EA_N, EB_N and EAB_N). In the first step, the carrier, E, can be facing the M or N side of the membrane, where either solute B or A can bind to the carrier so that the A-carrier complex (EA_M) and B-carrier complex (EB_N) are formed at opposite sides of the membrane. If the translocation of the formed complexes takes place, each of the complexes can undergo either a dissociation reaction or another binding reaction. If the dissociation reaction occurs, solute *A* will be released from the M face and solute *B* from the N surface of the membrane. If another binding reaction occurs, the complexes EAB_N and EAB_M will be formed at opposite sides of the membrane. Cha et al. (2009) developed a model for eight-state antiporter flux transport equations [136]; here, their model is reparametrized and transformed into the general resistance form. In this model, it is assumed that the dissociation constants for the binding reactions (association reactions) are not affected by the binding of A and B (that is, $K_{AB}^{MorN} = K_B^{MorN}$ and $K_{BA}^{MorN} = K_A^{MorN}$). It is also assumed that the carrier is non-symmetric, and that the binding reaction occurs much faster than the translocation steps (rapid binding assumption). Under these assumptions, the antiporter flux can be obtained via equation 62a and the transported fluxes of A and B are given by equations 62b and 62c, respectively.
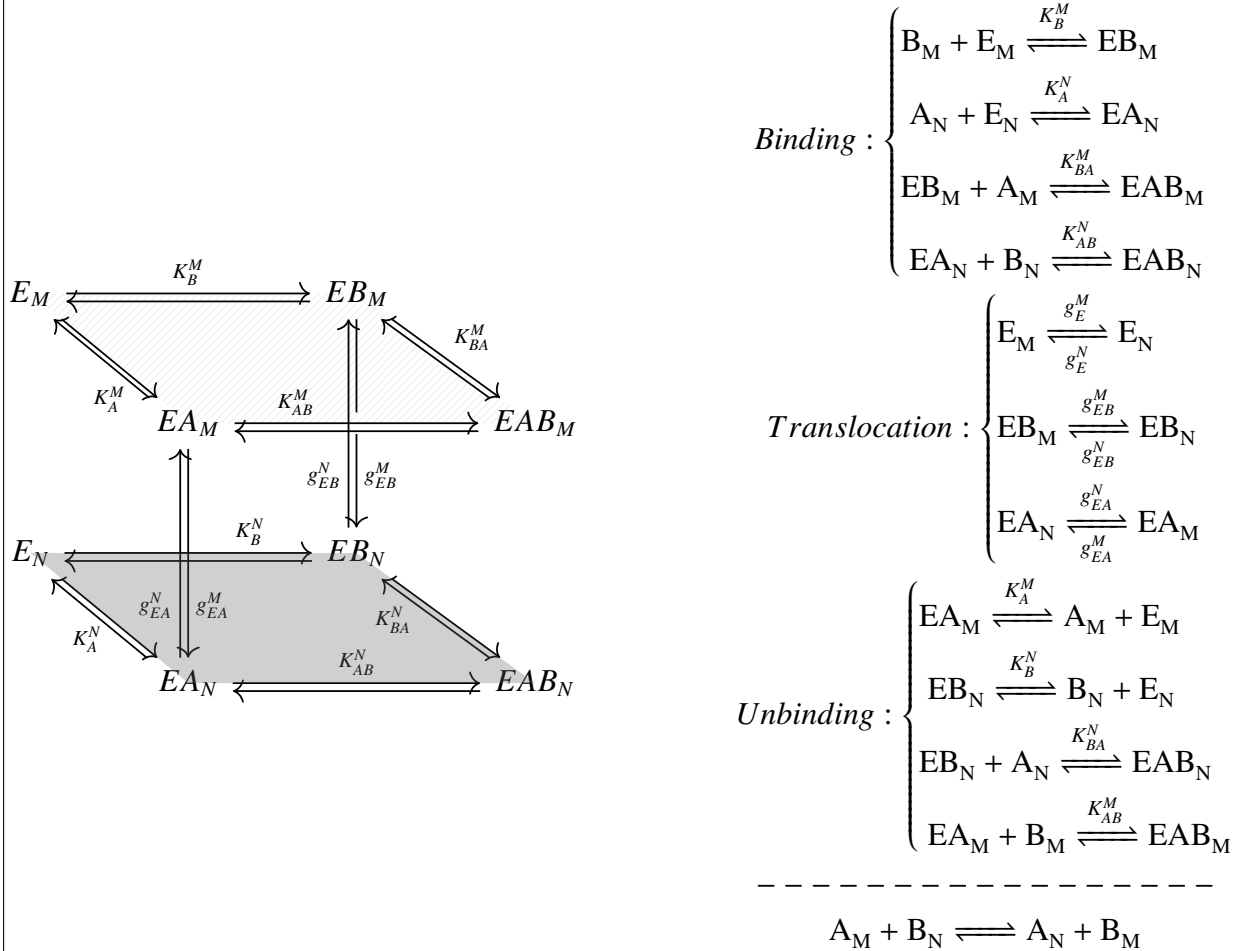
Figure 19: A schematic configuration of the antiporter eight-state transport mechanism and the resulting net transport flux equations. In developing this model, it is assumed that the dissociation constants for binding reactions are not affected by binding of A and B (which means to have $K_{AB}^{MorN} = K_B^{MorN}$ and $K_{BA}^{MorN} = K_A^{MorN}$). It is also assumed that: 1) the carrier is non-symmetric and 2) binding reaction occur much faster relative to the translocation of the carrier (rapid binding assumption) (part 1/2 continued on the next page).

$$J_{antiporter}^{M,N(net)} = [E]_t \frac{(g_{EA}^M \alpha^M)(g_{EB}^N \beta^N) - (g_{EA}^N \alpha^N)(g_{EB}^M \beta^M)}{R_M R_{NN} + R_N R_{MM}} \tag{62a}$$

$$J_{A,antiporter}^{M,N(net)} = [E]_t \frac{(g_{EA}^M \alpha^M)(g_{EB}^N \beta^N) - (g_{EA}^N \alpha^N)(g_{EB}^M \beta^M)}{R_M R_{NN} + R_N R_{MM}} \tag{62b}$$

$$J_{B,antiporter}^{M,N(net)} = [E]_t \frac{(g_{EB}^M \beta^M)(g_{EA}^N \alpha^N) - (g_{EB}^N \beta^N)(g_{EA}^M \alpha^M)}{R_M R_{NN} + R_N R_{MM}} \tag{62c}$$

where
$$[E]_t = [E]_M + [EA]_M + [EB]_M + [EAB]_M + [EAB]_N + [EB]_N + [EA]_N + [E]_N$$

$\alpha^M = \frac{[A]_M}{K_A^M}, \quad \beta^M = \frac{[B]_M}{K_B^M}$ $\qquad\qquad$ $\alpha^N = \frac{[A]_M}{K_A^N}, \quad \beta^N = \frac{[B]_N}{K_B^N}$

$R_M = 1 + \alpha^M + \beta^M + \alpha^M \beta^M$ $\qquad\qquad$ $R_N = 1 + \alpha^N + \beta^N + \alpha^N \beta^N$

$R_{MM} = g_{EA}^M \alpha^M + g_{EB}^M \beta^M$ $\qquad\qquad$ $R_{NN} = g_{EA}^N \alpha^N + g_{EB}^N \beta^N$
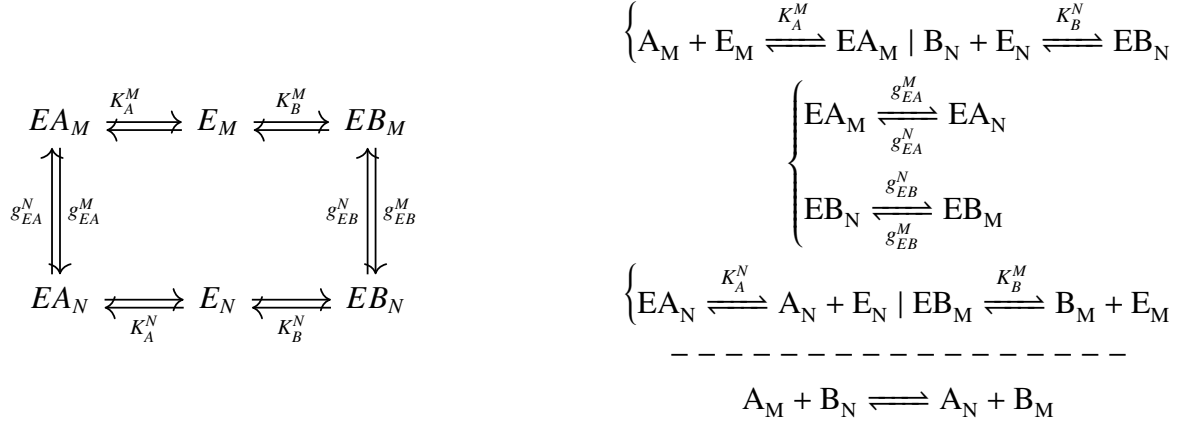
Figure 19: A schematic configuration of the antiporter eight-state transport mechanism and the resulting net transport flux equations. In developing this model, it is assumed that the dissociation constants for binding reactions are not affected by binding of A and B (which means to have $K_{AB}^{MorN} = K_B^{MorN}$ and $K_{BA}^{MorN} = K_A^{MorN}$). It is also assumed that: 1) the carrier is non-symmetric and 2) binding reaction occur much faster relative to the translocation of the carrier (rapid binding assumption) (part 2/2 continued from previous page).

Six-state antiporter ordered binding model:

The six-state model is very similar to the eight-state model, except that A and B cannot bind simultaneously to the transporter, and consequently, the formation of the complexes EAB_M and EAB_N does not occur. Figure 20 shows the "ping-pong" model of a six-state antiport transport model. As shown in Figure 20, in the first step, component A binds to the protein on the outside surface. Assuming that the binding of solute B to the carrier occurs simultaneously on the other side of the membrane, the A-carrier (EA_M) and B-carrier (EB_N) complexes are formed on opposite sides of the membrane. After translocation of the formed complexes, each of the complexes undergoes a dissociation reaction. These dissociation reactions lead to the release of solutes A and B from the N (inside) and M (outside) faces of the membrane, respectively. The A and B fluxes driven from region M to N via this antiport mechanism must be equal and opposite (i.e., $J_{B,antiporter}^{M,N} = -J_{A,antiporter}^{M,N}$). The six-state model was first developed by Weinstein et al. (2000)

[137] under the rapid binding assumption, i.e., the assumption that the solute binding and unbinding reactions at both sides of the membrane occur much faster than the translocation of the carrier complex. In this work, Stein's kinetic parameterization method is applied [131], and the transport fluxes are transformed into the resistance forms. The A and B fluxes are expressed in equations 63a and 63b, respectively.

Schematic configuration of the six-state antiporter ordered binding transport mechanism

$$EA_M \xrightleftharpoons{K_A^M} E_M \xrightleftharpoons{K_B^M} EB_M$$

$$g_{EA}^N \,\|\, g_{EA}^M \qquad\qquad g_{EB}^N \,\|\, g_{EB}^M$$

$$EA_N \xrightleftharpoons[K_A^N]{} E_N \xrightleftharpoons[K_B^N]{} EB_N$$

$$\left\{ A_M + E_M \xrightleftharpoons{K_A^M} EA_M \mid B_N + E_N \xrightleftharpoons{K_B^N} EB_N \right.$$

$$\left\{ \begin{aligned} EA_M &\xrightleftharpoons[g_{EA}^N]{g_{EA}^M} EA_N \\ EB_N &\xrightleftharpoons[g_{EB}^M]{g_{EB}^N} EB_M \end{aligned} \right.$$

$$\left\{ EA_N \xrightleftharpoons{K_A^N} A_N + E_N \mid EB_M \xrightleftharpoons{K_B^M} B_M + E_M \right.$$

- - - - - - - - - - - - - - - - - -

$$A_M + B_N \rightleftharpoons A_N + B_M$$

Net Transport Flux from M to N

$$J_{A,antiporter}^{M,N(net)} = [E]_t \frac{(g_{EA}^M \alpha^M)(g_{EB}^N \beta^N) - (g_{EA}^N \alpha^N)(g_{EB}^M \beta^M)}{R_M R_{NN} + R_N R_{MM}} \tag{63a}$$

$$J_{B,antiporter}^{M,N(net)} = [E]_t \frac{(g_{EB}^M \beta^M)(g_{EA}^N \alpha^N) - (g_{EB}^N \beta^N)(g_{EA}^M \alpha^M)}{R_M R_{NN} + R_N R_{MM}} \tag{63b}$$

where
$$[E]_t = [E]_M + [EA]_M + [EA]_N + [E]_N + [EB]_N + [EA]_N$$

$$\alpha^M = \frac{[A]_M}{K_A^M}, \qquad \beta^M = \frac{[B]_M}{K_B^M} \qquad\qquad \alpha^N = \frac{[A]_N}{K_A^N}, \qquad \beta^N = \frac{[B]_N}{K_B^N}$$

$$R_M = 1 + \alpha^M + \beta^M \qquad\qquad R_N = 1 + \alpha^N + \beta^N$$

$$R_{MM} = g_{EA}^M \alpha^M + g_{EB}^M \beta^M \qquad\qquad R_{NN} = g_{EA}^N \alpha^N + g_{EB}^N \beta^N$$

Figure 20: A schematic configuration of the antiporter six-state mechanism of two solutes and the regarding net flux transport equation. Transport equations are reparametrized and transformed into the general resistance form from Weinstein et al. (2000) model [137], the flux equations are transformed to the general form of the resistance terms. In developing this model, it is assumed that the dissociation constants for binding reactions is not affected by binding of A and B (which means to have $K_{AB}^{MorN} = K_B^{MorN}$ and $K_{BA}^{MorN} = K_A^{MorN}$). It is also assumed that: 1) the carrier is non-symmetric and 2) binding reaction occur much faster relative to the translocation of the carrier (rapid binding assumption).

Antiporter with competitor-ordered binding model:

Figure 21 shows a competitive antiporter transport model involving molecules of A, B, and C, in which C competes with B for the same binding sites on the carrier. In this configuration, A

578 flows from the M side to the N side, *B* moves in the opposite direction, and only the loaded

579 carrier can cross the membrane. Here, distinct affinities and dissociation constants at the two

580 sides of the membrane and for each of the solutes are considered, and the forward and backward

581 translocation rate constants of a given solute can differ. In this model, the rapid binding and

582 unbinding assumption and the quasi-steady-state assumption are used. Under these assumptions,

583 the outward fluxes for each of the solutes *A*, *B*, and *C* are obtained by equations 64a, 64b, and 64c,

584 respectively [100].

Schematic configuration of the antiporter with competitor-ordered binding transport mechanism

$$\begin{cases} A_M + E_M \underset{}{\overset{K_A^M}{\rightleftharpoons}} EA_M \\ C_N + E_N \underset{}{\overset{K_C^N}{\rightleftharpoons}} EC_N \\ B_N + E_N \underset{}{\overset{K_B^N}{\rightleftharpoons}} EB_N \end{cases}$$

$$\begin{cases} EA_M \underset{g_{EA}^N}{\overset{g_{EA}^M}{\rightleftharpoons}} EA_N \\ EC_N \underset{g_{EC}^M}{\overset{g_{EC}^N}{\rightleftharpoons}} EC_M \\ EB_N \underset{g_{EB}^M}{\overset{g_{EB}^N}{\rightleftharpoons}} EB_M \end{cases}$$

$$\begin{cases} EA_N \underset{}{\overset{K_A^N}{\rightleftharpoons}} E_N + A_N \\ EC_M \underset{}{\overset{K_C^M}{\rightleftharpoons}} E_M + C_M \\ EB_M \underset{}{\overset{K_B^M}{\rightleftharpoons}} E_M + B_M \end{cases}$$

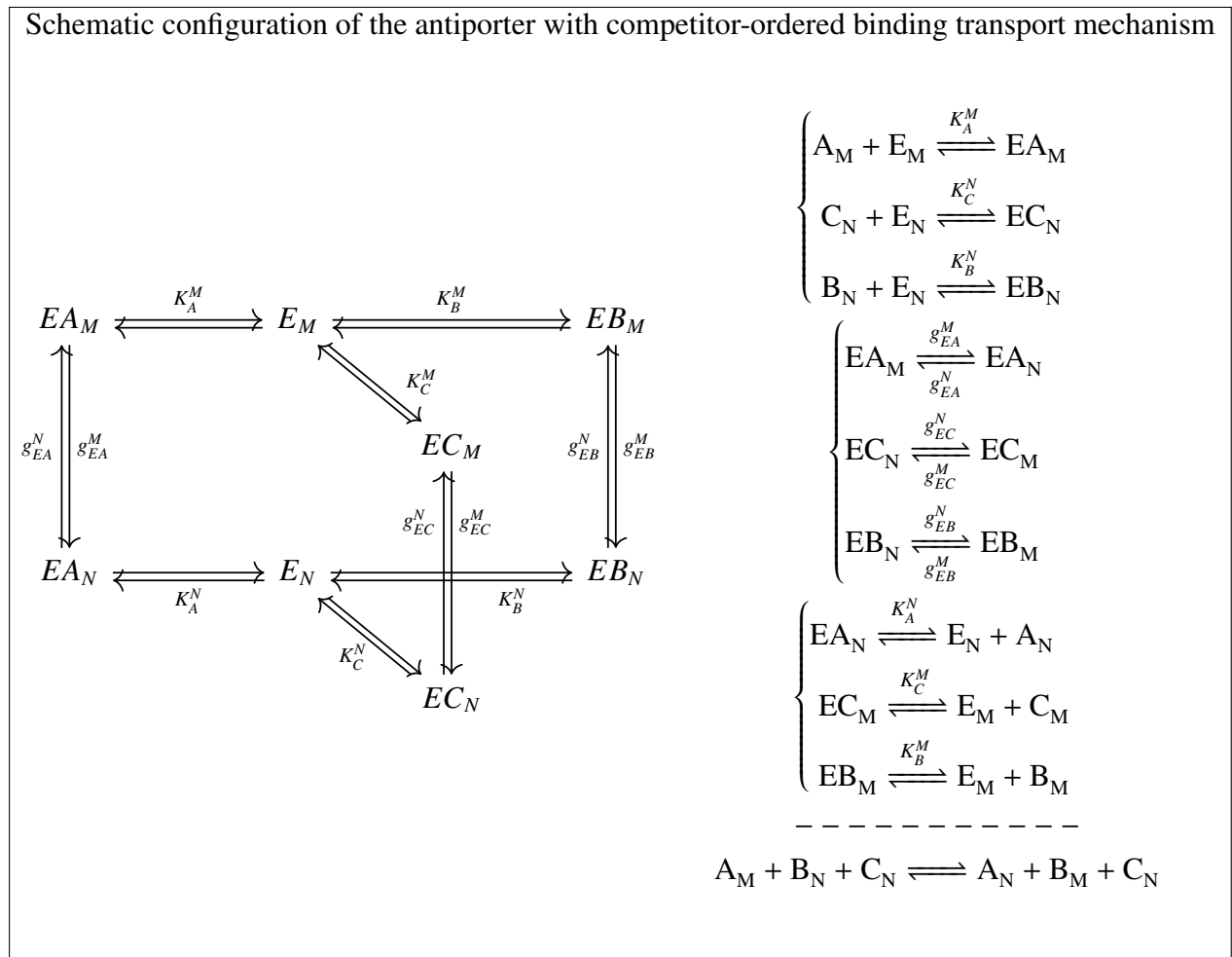$$A_M + B_N + C_N \rightleftharpoons A_N + B_M + C_N$$

Figure 21: A schematic configuration of the antiporter with competitor-ordered binding transport mechanism of two solutes and the regarding net transport flux equations. In this configuration, the carrier exists in four different states on each side of the membrane. Transport equations are reparameterized to the general model from Layton model [100]. Dissociation constants (K_A, K_B, and K_C terms), and the translocation rate constants (g_{EA}, g_{EB}, and g_{EC} terms) are depicted in the reaction cycle in the right panel. Subscripts M and N, denote the M and N sides of the membrane. $[E]_t$ is the total number of transporter per unit area of the membrane (part 1/2 continued on next page).

	Net Transport Fluxes	
	$$J_{A,antiporter}^{M,N(net)} = [E]_t \frac{g_{EA}^M \alpha^M (g_{EB}^N \beta^N + g_{EC}^N \gamma^N) - g_{EA}^N \alpha^N (g_{EB}^M \beta^M + g_{EC}^M \gamma^M)}{R_M R_{NN} + R_N R_{MM}}$$	(64a)
	$$J_{B,antiporter}^{M,N(net)} = [E]_t \frac{g_{EB}^M \beta^M (g_{EA}^N \alpha^N + g_{EC}^N \gamma^N) - g_{EB}^N \beta^N (g_{EA}^M \alpha^M + g_{EC}^M \gamma^M)}{R_M R_{NN} + R_N R_{MM}}$$	(64b)
	$$J_{C,antiporter}^{M,N(net)} = [E]_t \frac{g_{EC}^M \gamma^M (g_{EA}^N \alpha^N + g_{EB}^N \beta^N) - g_{EC}^N \gamma^N (g_{EA}^M \alpha^M + g_{EB}^M \beta^M)}{R_M R_{NN} + R_N R_{MM}}$$	(64c)

where
$$[E]_t = [E]_M + [EA]_M + [EB]_M + [EC]_M + [E]_N + [EA]_N + [EB]_N + [EC]_N$$

$\alpha^M = \frac{[A]_M}{K_A^M}, \quad \beta^M = \frac{[B]_M}{K_B^M}, \quad \gamma^M = \frac{[C]_M}{K_C^M}$ $\qquad$ $\alpha^N = \frac{[A]_N}{K_A^N}, \quad \beta^N = \frac{[B]_N}{K_B^N}, \quad \gamma^N = \frac{[C]_N}{K_C^N}$

$R_M = 1 + \alpha^M + \beta^M + \gamma^M$ $\qquad\qquad\qquad$ $R_N = 1 + \alpha^N + \beta^N + \gamma^N$

$R_{MM} = g_{EA}^M \alpha^M + g_{EB}^M \beta^M + g_{EC}^M \gamma^M$ $\qquad$ $R_{NN} = g_{EA}^N \alpha^N + g_{EB}^N \beta^N + g_{EC}^N \gamma^N$

Figure 21: A schematic configuration of the antiporter with competitor-ordered binding transport mechanism of two solutes and the regarding net transport flux equations. In this configuration, the carrier exists in four different states on each side of the membrane. Transport equations are reparametrized and transformed into the general resistance form from Layton model [100]. Dissociation constants (K_A, K_B, and K_C terms), and the translocation rate constants (g_{EA}, g_{EB}, and g_{EC} terms) are depicted in the reaction cycle in the right panel. Subscripts M and N, denote the M and N sides of the membrane. $[E]_t$ is the total number of transporter per unit area of the membrane (part 2/2 continued from previous page).

Antiporter simplified model:

Simplified models of antiport and symport transporters have been developed using similar assumptions. Sohma et al. (1996) developed a simplified antiporter model for the one-to-one transport of two substrates [138]. Here, their model is extended to the general case of an antiporter transporting three solutes in a ratio of $aA : bB : cC$. The following assumptions are used: 1) the rapid binding and unbinding assumption, 2) the quasi-steady-state assumption, and 3) the symmetric carrier assumption (i.e., the velocity constants $g_{antiporter}$ for transport from the M to the N side of the membrane vice-versa are the same, $g_{EA}^M = g_{EA}^N = g_{antiporter}$, and the dissociation constants for each solute on both faces are the same, $K_A^M = K_A^N = K_A$, $K_B^M = K_B^N = K_B$), 4) the antiporter has a single binding site for the transported solutes, 5) the transported solutes compete for the same binding sites, and 6) finally, the empty antiporter does not cross the membrane. Using these as-

sumptions, the steady-state turnover rate of the exchanger can be derived from equation 65a, and the corresponding fluxes of substrates A, B, and C are obtained through equations 65b, 65c, and 65d, respectively.

<div style="border:1px solid black">

A general simplified antiporter transport with three substrates

$$aA_M + bB_N + cC_N \rightleftharpoons aA_N + bB_M + cC_M$$

Net Transport Flux from M to N

$$J^{M,N(net)}_{antiporter} = P_{antiporter} \frac{(\alpha^M)^a (\beta^N)^b (\gamma^N)^c - (\alpha^N)^a (\beta^M)^b (\gamma^M)^c}{R'_M R'_{NN} + R'_N R'_{MM}} \tag{65a}$$

$$J^{M,N(net)}_{A,antiporter} = a J^{M,N(net)}_{antiporter} \tag{65b}$$

$$J^{M,N(net)}_{B,antiporter} = b J^{M,N}_{antiporter} \tag{65c}$$

$$J^{M,N(net)}_{C,antiporter} = c J^{M,N(net)}_{antiporter} \tag{65d}$$

where $P_{antiporter} = [E]_t g_{antiporter}$ describes the membrane permeability to the antiporter, and the thermodynamic parameters and resistances are defined as:

$$\alpha^M = \frac{[A]_M}{K_A}, \quad \beta^M = \frac{[B]_M}{K_B}, \quad \gamma^M = \frac{[C]_M}{K_C}$$
$$R'_M = (1 + \alpha^M)^a (1 + \beta^M)^b (1 + \gamma^M)^c$$
$$R'_{MM} = (a\alpha^M + b\beta^M + c\gamma^M)$$

$$\alpha^N = \frac{[A]_N}{K_A}, \quad \beta^N = \frac{[B]_N}{K_B}, \quad \gamma^N = \frac{[C]_N}{K_C}$$
$$R'_N = (1 + \alpha^N)^a (1 + \beta^N)^b (1 + \gamma^N)^c$$
$$R'_{NN} = (a\alpha^N + b\beta^N + c\gamma^N)$$

</div>

Figure 22: Antiporter Simplified Model. The following assumptions are used: (1) the rapid binding and unbind assumptions, (2) the quasi-steady-state assumption, (3) similarity assumption for all rate constants (4) antiporter has a single site which bound the transported solute (5) the transported solute competed for the same binding sites (6) finally, the empty antiporter does not cross the membrane.

6. Discussion and Conclusion

Multiscale mathematical modeling of biological transport mechanisms in the human body has advanced significantly over the last few decades. Simultaneous advances in experimental techniques and computational power have produced models with much greater predictive power, complexity, and usefulness; these models can be used to achieve a more thorough understanding of membrane physiology and disorders. These advances have also led to new techniques in the pre-

vention, diagnosis, and treatment of diseases caused by membrane disorders. This work focused on compiling the mathematical models that have been developed for biological transport in tissue compartments. The tissue volume was divided into five different compartments, including the capillary, interstitial region, cell membrane, intracellular space, and duct lumen. Next, mass transport models for fluids and solutes *within* and *across* the walls of these compartments were described. These transport mechanisms include diffusion, convection, migration, and membrane-mediated transport mechanisms (channels, uniporters, ATPase pumps, symporters, and antiporters). One or more of these mass transport mechanisms may occur in each of the five compartments. In capillaries and ducts, convection is the dominant mechanism of solute transport within these compartments [139, 140], and filtration (or hindered convection) is the controlling transport mechanism for fluid flow across their walls [141–143]. Transport within the interstitial matrix occurs mainly via the diffusion mechanism. Mass transport across the cell membrane occurs via diffusion, filtration, water channels, various ion channels, and different families of transporters such as pumps, symporters, and antiporters.

The mathematical models describing these transport mechanisms were discussed, and the terminology used for the fundamental concepts of these models was highlighted. The membrane carriers and ion channels were a particular focus. Both detailed and simplified models were provided for the former. Depending on the purpose of the study, one or more of these models can be applied. As discussed earlier, the physics underlying most of these models is similar; the differences among them arise from the binding and unbinding order of the solutes and the assumptions applied for various reaction steps. The basic building blocks of the transport process include the diffusion, convection, and migration mechanisms. These three transport mechanisms occur along an existing gradient (e.g., a pressure, chemical, or electrochemical gradient), and their models require physical parameters such as hydraulic conductance, permeability, diffusion coefficients, viscosity, and mobility. For the convection mechanism, the existing pressure gradients play a controlling role, and the associated parameters are the solute sieving coefficient and hydraulic conductance of the solvent. Diffusion and migration are driven by chemical and electrochemical gradients; the main physical parameters of these processes are the diffusion coefficient and the electrokinetic mobility, respectively. Other transport mechanisms can be expressed as combinations of the

59

main transport mechanisms and using the kinetic reaction equations (the mass-action kinetic, Hill model, and Michaelis-Menten equations); depending on the type of transport, one or more of these equations will be applicable. For example, water channels are modeled as a combination of the diffusion and filtration equations. In the same fashion, the combination of diffusion and migration equations can be used to model the ionic current through the ion channels, which leads to the non-linear Goldman-Hodgkin-Katz model. The linear Ohmic model can also be applied to derive the current through ion channels. In the Ohmic model, the parameters are the membrane electric conductance towards the specific ion of interest and the density of ion channels per unit membrane. Carrier-mediated transport mechanisms are based on a different modeling approach. Since these transporters are fixed within the membrane, they are described merely by using kinetic reaction equations, and the thermal behavior of the transporting molecules is captured in the reaction rate coefficients. These models are experimentally traceable, which allows them to be used as reflective tools for examining the behavior of the transporters and making predictions. Therefore, to model multi-step transporter mechanisms, interpolation of the kinetic data is needed. To facilitate the selection of the appropriate kinetic model for transforming the experimentally obtained kinetic data to the appropriate mathematical model, these transporters were categorized into various groups, and appropriate models for quantitative description of their function were provided.

The development of models at each scale has been achieved by substantial efforts of several established research experts in the interdisciplinary research area of biological mass transport mechanisms. It is not possible to acknowledge or discuss all the research endeavors in different fields in this research area. The comprehensive overview completed in this work represents an attempt to compile the relevant terminology and the developed mass transport mathematical models in biological systems, which have resulted from various lines of research expertise, in a single paper. These contemporary theories and modeling techniques will provide essential knowledge and bridge the gap between physiologists, biophysicists, and engineers interested in modeling biological mass transport processes. Finally, as modeling becomes more prevalent, there is still a need to ensure that the proper physics assumptions are elucidated and considered, and that new modeling methodologies and simplifications are directed towards the key issues. Thus, there remain significant issues that require more research and understanding. While our study was not

designed to address the potential issues of currently available models, we hope that researchers can use this work as additional tool to improve the accuracy of the existing models and generate novel models, which in turn could lead to critical discoveries in the important areas of health, pathology, medicine, and membrane disease.

Declaration of Competing Interest

There are no conflicts of interest to declare.

Funding

Acknowledgment

References

[1] D. Moulton, V. Sulzer, G. Apodaca, H. Byrne, S. Waters, Mathematical modelling of stretch-induced membrane traffic in bladder umbrella cells, Journal of theoretical biology 409 (2016) 115–132.

[2] E. Drioli, M. Nakagaki, Membranes and membrane processes, Springer Science & Business Media, 2013.

[3] W. Ang, A. W. Mohammad, Mathematical modeling of membrane operations for water treatment, in: Advances in Membrane Technologies for Water Treatment, Elsevier, 2015, pp. 379–407.

[4] N. V. Mantzaris, S. Webb, H. G. Othmer, Mathematical modeling of tumor-induced angiogenesis, Journal of mathematical biology 49 (2) (2004) 111–187.

[5] A. Beicha, R. Zaamouche, Mathematical Modeling of Flux in Ultrafiltration Membrane, Recent Patents on Chemical Engineering 5 (2) (2012) 110–115.

[6] H. S. Silva, A. Kapela, N. M. Tsoukias, A mathematical model of plasma membrane electrophysiology and calcium dynamics in vascular endothelial cells, American Journal of Physiology-Cell Physiology 293 (1) (2007) C277–C293.

[7] R. A. Devenyi, F. A. Ortega, W. Groenendaal, T. Krogh-Madsen, D. J. Christini, E. A. Sobie, Differential roles of two delayed rectifier potassium currents in regulation of ventricular action potential duration and arrhythmia susceptibility, The Journal of physiology 595 (7) (2017) 2301–2317.

[8] M. Ursino, E. Magosso, Acute cardiovascular response to isocapnic hypoxia. i. a mathematical model, American Journal of Physiology-Heart and Circulatory Physiology 279 (1) (2000) H149–H165.

[9] A. T. Fojo, E. A. Kendall, P. Kasaie, S. Shrestha, T. A. Louis, D. W. Dowdy, Mathematical Modeling of "Chronic" Infectious diseases: Unpacking the black box, in: Open forum infectious diseases, Vol. 4, Oxford University Press US, 2017, p. ofx172.

[10] L. Edelstein-Keshet, Mathematical models in biology, SIAM, 2005.

[11] J. D. Murray, Mathematical biology II, Vol. 2, springer, 2002.

[12] L. Geris, et al., Computational modeling in tissue engineering, Springer, 2013.

[13] V. C. Rideout, Mathematical and computer modeling of physiological systems, Prentice Hall Englewood Cliffs, NJ:, 1991.

[14] W. Stillwell, An introduction to biological membranes: from bilayers to rafts, Newnes, 2013.

[15] P. L. Yeagle, The membranes of cells, Academic Press, 2016.

[16] J. J. Batzel, M. Bachar, F. Kappel, Mathematical modeling and validation in physiology: applications to the cardiovascular and respiratory systems, Vol. 2064, Springer, 2012.

[17] J. J. Feher, Quantitative human physiology: an introduction, Academic press, 2017.

[18] R. I. Macey, Mathematical models of membrane transport processes, in: Physiology of membrane disorders, Springer, 1986, pp. 111–131.

[19] J. P. Keener, J. Sneyd, Mathematical physiology, Vol. 1, Springer, 1998.

[20] S. Motta, F. Pappalardo, Mathematical modeling of biological systems., Briefings in bioinformatics 14 (4) (2013) 411–22. doi:10.1093/bib/bbs061.

[21] R. Martin, M. Fisher, R. Minchin, K. Teo, A mathematical model of cancer chemotherapy with an optimal selection of parameters, Mathematical biosciences 99 (2) (1990) 205–230.

[22] Z. Liu, C. Yang, A mathematical model of cancer treatment by radiotherapy followed by chemotherapy, Mathematics and Computers in Simulation 124 (2016) 1–15.

[23] S. Khadraoui, F. Harrou, H. N. Nounou, M. N. Nounou, A. Datta, S. P. Bhattacharyya, A measurement-based control design approach for efficient cancer chemotherapy, Information Sciences 333 (2016) 108–125.

[24] H. Moradi, G. Vossoughi, H. Salarieh, Optimal robust control of drug delivery in cancer chemotherapy: a comparison between three control approaches, Computer methods and programs in biomedicine 112 (1) (2013) 69–83.

[25] T. Sund, A mathematical model for counter-current multiplications in the swim-bladder., The Journal of physiology 267 (3) (1977) 679–696.

[26] D.-M. Oh, H.-k. Han, G. L. Amidon, Drug transport and targeting, in: Membrane transporters as drug targets, Springer, 2002, pp. 59–88.

[27] S. Brady, G. Siegel, R. W. Albers, D. Price, Basic neurochemistry: principles of molecular, cellular, and

724   medical neurobiology, Academic press, 2011.

725   [28] M. Almog, A. Korngreen, Is realistic neuronal modeling realistic?, Journal of neurophysiology 116 (5) (2016)
726   2180–2209.

727   [29] A. Farghadan, A. Arzani, The combined effect of wall shear stress topology and magnitude on cardiovascular
728   mass transport, International Journal of Heat and Mass Transfer 131 (2019) 252–260.

729   [30] R. Klabunde, Cardiovascular physiology concepts, Lippincott Williams & Wilkins, 2011.

730   [31] F. M. Melchior, R. S. Srinivasan, J. B. Charles, Mathematical modeling of human cardiovascular system for
731   simulation of orthostatic response, American Journal of Physiology-Heart and Circulatory Physiology 262 (6)
732   (1992) H1920–H1933.

733   [32] A. Albanese, L. Cheng, M. Ursino, N. W. Chbat, An integrated mathematical model of the human car-
734   diopulmonary system: model development, American Journal of Physiology-Heart and Circulatory Physiology
735   310 (7) (2015) H899–H921.

736   [33] J. Xi, P. W. Longest, Numerical predictions of submicrometer aerosol deposition in the nasal cavity using a
737   novel drift flux approach, International Journal of Heat and Mass Transfer 51 (23-24) (2008) 5562–5577.

738   [34] G. Nucci, C. Cobelli, Mathematical models of respiratory mechanics, in: Modeling methodology for physiol-
739   ogy and medicine, Elsevier, 2001, pp. 279–304.

740   [35] L. Mao, H. Udaykumar, J. Karlsson, Simulation of micro-scale interaction between ice and biological cells,
741   International journal of heat and mass transfer 46 (26) (2003) 5123–5136.

742   [36] L. G. Palmer, Epithelial transport in The Journal of General Physiology, The Journal of general physiology
743   149 (10) (2017) 897–909.

744   [37] J. M. Han, V. Periwal, A mathematical model of calcium dynamics: Obesity and mitochondria-associated ER
745   membranes, bioRxiv (2018) 477968.

746   [38] B. Binder, A. Goede, N. Berndt, H.-G. Holzhütter, A conceptual mathematical model of the dynamic self-
747   organisation of distinct cellular organelles, PloS one 4 (12) (2009) e8295.

748   [39] A. K. Babcock, T. Q. Garvey, M. Berman, A mathematical model for membrane transport of amino acid and
749   Na+ in vesicles, The Journal of membrane biology 49 (2) (1979) 157–169.

750   [40] J. Mikekisz, J. Gomulkiewicz, S. Miekisz, Mathematical models of ion transport through cell membrane chan-
751   nels, Mathematica Applicanda 42 (1) (2014) 39–62.

752   [41] E. Gin, E. J. Crampin, D. A. Brown, T. J. Shuttleworth, D. I. Yule, J. Sneyd, A mathematical model of fluid
753   secretion from a parotid acinar cell, Journal of theoretical biology 248 (1) (2007) 64–80.

754   [42] N. Alaa, H. Lefraich, Computational simulation of a new system modelling ions electromigration through
755   biological membranes, Theoretical Biology and Medical Modelling 10 (1) (2013) 51.

756   [43] K. Vafai, Handbook of porous media, Crc Press, 2015.

757   [44] V. R. Voller, A. Brent, C. Prakash, The modelling of heat, mass and solute transport in solidification systems,

International Journal of Heat and Mass Transfer 32 (9) (1989) 1719–1731.

[45] W. Liu, G. Zhao, Z. Shu, T. Wang, K. Zhu, D. Gao, High-precision approach based on microfluidic perfusion chamber for quantitative analysis of biophysical properties of cell membrane, International Journal of Heat and Mass Transfer 86 (2015) 869–879.

[46] K. Cook, A. Marafie, et al., The role of porous media in modeling fluid flow within hollow fiber membranes of the total artificial lung, Journal of porous media 15 (2) (2012).

[47] K. Vafai, Porous media: applications in biological systems and biotechnology, CRC Press, 2010.

[48] L. Wang, L.-P. Wang, Z. Guo, J. Mi, Volume-averaged macroscopic equation for fluid flow in moving porous media, International Journal of Heat and Mass Transfer 82 (2015) 357–368.

[49] J. S. Ultman, H. Baskaran, G. M. Saidel, Biomedical Mass Transport and Chemical Reaction: Physicochemical Principles and Mathematical Modeling, John Wiley & Sons, 2016.

[50] D. A. Nield, A. Bejan, et al., Convection in porous media, Vol. 3, Springer, 2006.

[51] R. B. Bird, Transport phenomena, Applied Mechanics Reviews 55 (1) (2002) R1–R4.

[52] C. G. Hill, T. W. Root, An introduction to chemical engineering kinetics & reactor design, Wiley Online Library, 1977.

[53] S. Becker, Modeling of Microscale Transport in Biological Processes, Academic Press, 2016.

[54] J. Pallares, J. A. Ferré, A simple model to predict mass transfer rates and kinetics of biochemical and biomedical Michaelis–Menten surface reactions, International Journal of Heat and Mass Transfer 80 (2015) 192–198.

[55] J. S. Lolkema, D.-J. Slotboom, The hill analysis and co-ion–driven transporter kinetics, The Journal of general physiology 145 (6) (2015) 565–574.

[56] J. N. Weiss, The hill equation revisited: uses and misuses., The FASEB Journal 11 (11) (1997) 835–841.

[57] O. Yifrach, Hill coefficient for estimating the magnitude of cooperativity in gating transitions of voltage-dependent ion channels, Biophysical journal 87 (2) (2004) 822–830.

[58] C. Loudon, K. McCulloh, Application of the Hagen-Poiseuille Equation to Fluid Feeding through Short Tubes, Annals of the Entomological Society of America 92 (1) (1999) 153–158.

[59] B. Pirofsky, The determination of blood viscosity in man by a method based on Poiseuille's law, The Journal of clinical investigation 32 (4) (1953) 292–298.

[60] S. Singh, L. V. Randle, P. T. Callaghan, C. J. Watson, C. J. Callaghan, Beyond Poiseuille: preservation fluid flow in an experimental model, Journal of transplantation 2013 (2013).

[61] R. L. Fournier, Basic transport phenomena in biomedical engineering, CRC press, 2017.

[62] M. Khakpour, K. Vafai, Critical assessment of arterial transport models, International Journal of Heat and Mass Transfer 51 (3-4) (2008) 807–822.

[63] W. Gösele, C. Alt, Filtration, Ullmann's Encyclopedia of Industrial Chemistry (2005).

[64] L. Costanzo, Physiology Cases and Problems, Lippincott Williams & Wilkins, 2012.

[65] C. J. Geankoplis, Transport processes and separation process principles:(includes unit operations), Prentice Hall Professional Technical Reference, 2003.

[66] L. Luo, B. Yu, J. Cai, M. Mei, Symmetry is not always prefect, International Journal of Heat and Mass Transfer 53 (21-22) (2010) 5022–5024.

[67] E. M. Renkin, Filtration, diffusion, and molecular sieving through porous cellulose membranes, The Journal of general physiology 38 (2) (1954) 225–243.

[68] J. S. Schultz, R. Valentine, C. Y. Choi, Reflection coefficients of homopore membranes: effect of molecular size and configuration., The Journal of general physiology 73 (1) (1979) 49–60.

[69] B. Åberg, J. V. Hägglund, A Convection-Diffusion Model of Capillary Permeability with Reference to Single-injection Experiments, Upsala journal of medical sciences 79 (1) (1974) 7–17.

[70] M. Kojic, M. Milosevic, N. Kojic, Z. Starosolski, K. Ghaghada, R. Serda, A. Annapragada, M. Ferrari, A. Ziemys, A multi-scale FE model for convective–diffusive drug transport within tumor and large vascular networks, Computer Methods in Applied Mechanics and Engineering 294 (2015) 100–122.

[71] J. Lu, W.-Q. Lu, A numerical simulation for mass transfer through the porous membrane of parallel straight channels, International Journal of Heat and Mass Transfer 53 (11-12) (2010) 2404–2413.

[72] B. Rippe, M. Townsley, J. Parker, A. Taylor, Osmotic reflection coefficient for total plasma protein in lung microvessels, Journal of Applied Physiology 58 (2) (1985) 436–442.

[73] L. J. Groome, G. T. Kinasemitz, J. N. Diana, Diffusion and convection across heteroporous membranes: A simple macroscopic equation, Microvascular research 26 (3) (1983) 307–322.

[74] S. M. Hassanizadeh, Derivation of basic equations of mass transport in porous media, part 2. Generalized Darcy's and Fick's laws, Advances in water resources 9 (4) (1986) 207–222.

[75] C. Wilke, P. Chang, Correlation of diffusion coefficients in dilute solutions, AIChE Journal 1 (2) (1955) 264–270.

[76] E. Nagy, Basic equations of the mass transport through a membrane layer, Elsevier, 2012.

[77] P. Bordat, F. Affouard, M. Descamps, F. Müller-Plathe, The breakdown of the Stokes–Einstein relation in supercooled binary liquids, Journal of Physics: Condensed Matter 15 (32) (2003) 5397.

[78] H. L. Weissberg, Effective diffusion coefficient in porous media, Journal of Applied Physics 34 (9) (1963) 2636–2639.

[79] H.-h. Chen, H. Shen, S. Heimfeld, K. K. Tran, J. Reems, A. Folch, D. Gao, A microfluidic study of mouse dendritic cell membrane transport properties of water and cryoprotectants, International Journal of Heat and Mass Transfer 51 (23-24) (2008) 5687–5694.

[80] W. Shinoda, Permeability across lipid membranes, Biochimica et Biophysica Acta (BBA)-Biomembranes 1858 (10) (2016) 2254–2265.

[81] J. Newman, The effect of migration in laminar diffusion layers, International Journal of Heat and Mass Transfer

826   10 (7) (1967) 983–997.

827 [82] N. Ibl, Fundamentals of transport phenomena in electrolytic systems, in: Comprehensive treatise of electro-
828   chemistry, Springer, 1983, pp. 1–63.

829 [83] N. J. Yang, M. J. Hinner, Getting across the cell membrane: an overview for small molecules, peptides, and
830   proteins, Site-Specific Protein Labeling: Methods and Protocols (2015) 29–53.

831 [84] D. L. Nelson, A. L. Lehninger, M. M. Cox, Lehninger principles of biochemistry, Macmillan, 2008.

832 [85] R. Funk, Ion gradients in tissue and organ biology, Biol. Syst. Open Access 2 (2) (2013) 10–4172.

833 [86] R. Krämer, C. Ziegler, Membrane Transport Mechanism: 3D Structure and Beyond, Vol. 17, Springer Science
834   & Business Media, 2014.

835 [87] C. Peracchia, Handbook of membrane channels: molecular and cellular physiology, Academic Press, 2012.

836 [88] Q. Yan, Membrane transporters: methods and protocols, Vol. 227, Springer Science & Business Media, 2003.

837 [89] M. A. Hediger, M. F. Romero, J.-B. Peng, A. Rolfs, H. Takanaga, E. A. Bruford, The abcs of solute carri-
838   ers: physiological, pathological and therapeutic implications of human membrane transport proteins, Pflügers
839   Archiv 447 (5) (2004) 465–468.

840 [90] S. G. Dahl, I. Sylte, A. W. Ravna, Structures and models of transporter proteins, Journal of Pharmacology and
841   Experimental Therapeutics 309 (3) (2004) 853–860.

842 [91] G. Wisedchaisri, S. L. Reichow, T. Gonen, Advances in structural and functional analysis of membrane proteins
843   by electron crystallography, Structure 19 (10) (2011) 1381–1393.

844 [92] D. L. Theobald, C. Miller, Membrane transport proteins: surprises in structural sameness, Nature Structural
845   and Molecular Biology 17 (1) (2010) 2.

846 [93] K. Venko, A. R. Choudhury, M. Novič, Computational approaches for revealing the structure of membrane
847   transporters: case study on bilitranslocase, Computational and structural biotechnology journal 15 (2017) 232–
848   242.

849 [94] S. P. Alexander, E. Kelly, N. V. Marrion, J. A. Peters, E. Faccenda, S. D. Harding, A. J. Pawson, J. L. Sharman,
850   C. Southan, J. A. Davies, et al., The concise guide to pharmacology 2017/18: other ion channels, British journal
851   of pharmacology 174 (2017) S195–S207.

852 [95] B. Alberts, D. Bray, K. Hopkin, A. D. Johnson, J. Lewis, M. Raff, K. Roberts, P. Walter, Essential cell biology,
853   Garland Science, 2015.

854 [96] C. Maffeo, S. Bhattacharya, J. Yoo, D. Wells, A. Aksimentiev, Modeling and simulation of ion channels,
855   Chemical reviews 112 (12) (2012) 6250–6284.

856 [97] V. Salari, H. Naeij, A. Shafiee, Quantum Interference and Selectivity through Biological Ion Channels, Scien-
857   tific Reports 7 (2017) 41625.

858 [98] S. Yesylevskyy, V. Kharkyanen, Hierarchy of Motions and Quasi-Particles in a Simplified model of Potassium
859   Channel Selectivity Filter, Journal of biological physics 30 (2) (2004) 187–201.

66

[99] S. R. Mathur, J. Y. Murthy, A multigrid method for the Poisson-Nernst-Planck equations, International Journal of Heat and Mass Transfer 52 (17-18) (2009) 4031– 4039.

[100] A. T. Layton, A. Edwards, Mathematical Modeling in Renal Physiology, Springer, 2014.

[101] J. D. Stockand, M. S. Shapiro, Ion channels: methods and protocols, Vol. 337, Springer Science & Business Media, 2006.

[102] B. Hille, et al., Ion channels of excitable membranes, Vol. 507, Sinauer Sunderland, MA, 2001.

[103] J. Zheng, M. C. Trudeau, Handbook of ion channels, CRC Press, 2015.

[104] B. Hille, Ionic channels in excitable membranes. current problems and biophysical approaches, Biophysical Journal 22 (2) (1978) 283–294.

[105] A. L. Hodgkin, A. F. Huxley, A quantitative description of membrane current and its application to conduction and excitation in nerve, The Journal of physiology 117 (4) (1952) 500–544.

[106] C. M. Armstrong, The Na/K pump, Cl ion, and osmotic stabilization of cells, Proceedings of the National Academy of Sciences 100 (10) (2003) 6257–6262.

[107] C. V. Falkenberg, J. G. Georgiadis, Water and solute active transport through human epidermis: contribution of electromigration, International Journal of Heat and Mass Transfer 51 (23-24) (2008) 5623–5632.

[108] A. Hill, Fluid transport: a guide for the perplexed, Journal of Membrane Biology 223 (1) (2008) 1–11.

[109] K. Takata, T. Matsuzaki, Y. Tajika, Aquaporins: water channel proteins of the cell membrane, Progress in histochemistry and cytochemistry 39 (1) (2004) 1–83.

[110] A. Verkman, Aquaporins in clinical medicine, Annual review of medicine 63 (2012) 303–316.

[111] M. C. Papadopoulos, S. Saadoun, Key roles of aquaporins in tumor biology, Biochimica et Biophysica Acta (BBA)-Biomembranes 1848 (10) (2015) 2576–2583.

[112] R. E. Day, P. Kitchen, D. S. Owen, C. Bland, L. Marshall, A. C. Conner, R. M. Bill, M. T. Conner, Human aquaporins: regulators of transcellular water flow, Biochimica et Biophysica Acta (BBA)-General Subjects 1840 (5) (2014) 1492–1506.

[113] J. M. Carbrey, P. Agre, Discovery of the aquaporins and development of the field, in: Aquaporins, Springer, 2009, pp. 3–28.

[114] N. C. de Lanerolle, T.-S. Lee, D. D. Spencer, Astrocytes and epilepsy, Neurotherapeutics 7 (4) (2010) 424–438.

[115] K. Tani, Y. Fujiyoshi, Water channel structures analysed by electron crystallography, Biochimica et Biophysica Acta (BBA)-General Subjects 1840 (5) (2014) 1605–1613.

[116] K. Alleva, O. Chara, G. Amodeo, Aquaporins: another piece in the osmotic puzzle, FEBS letters 586 (19) (2012) 2991–2999.

[117] O. Kedem, A. Katchalsky, Thermodynamic analysis of the permeability of biological membranes to non-electrolytes, Biochimica et biophysica Acta 27 (1958) 229–246.

[118] H. Y. Elmoazzen, J. A. Elliott, L. E. McGann, Osmotic transport across cell membranes in nondilute solutions:

894   a new nondilute solute transport equation, Biophysical journal 96 (7) (2009) 2559–2571.

895 [119] E. Landis, Exchange of substances through the capillary walls, Handbook of Physiology, circulation II (1963)
896   961–1034.

897 [120] J. Mitchell, R. Schmidt, J. Shepherd, F. Abboud, Handbook of physiology, section 2: The cardiovascular
898   system, vol. 3. Peripheral circulation and organ blood flow, Oxford University Press, 1983.

899 [121] S. Barclay, D. Bennett, The direct measurement of plasma colloid osmotic pressure is superior to colloid
900   osmotic pressure derived from albumin or total protein, Intensive care medicine 13 (2) (1987) 114–118.

901 [122] J. S. Schultz, J. D. Goddard, S. R. Suchdeo, Facilitated transport via carrier-mediated diffusion in membranes:
902   Part i. Mechanistic aspects, experimental systems and characteristic regimes, AIChE Journal 20 (3) (1974)
903   417–445.

904 [123] A. S. Popel, J. D. Hellums, Theory of oxygen transport to tissue, Critical reviews in biomedical engineering
905   17 (3) (1989) 257.

906 [124] E. Cussler, R. Aris, A. Bhown, On the limits of facilitated diffusion, Journal of membrane science 43 (2-3)
907   (1989) 149–164.

908 [125] J. E. Darnell, H. F. Lodish, D. Baltimore, et al., Molecular cell biology, Vol. 2, Scientific American Books New
909   York, 1990.

910 [126] S. A. Shaikh, P.-C. Wen, G. Enkavi, Z. Huang, E. Tajkhorshid, Capturing functional motions of membrane
911   channels and transporters with molecular dynamics simulation, Journal of computational and theoretical
912   nanoscience 7 (12) (2010) 2481–2500.

913 [127] A. Katzir-Katchalsky, P. F. Curran, Nonequilibrium thermodynamics in biophysics, Harvard University Press,
914   1965.

915 [128] A. Kleinzeller, D. J. Benos, M. J. Caplan, Cell Biology and Membrane Transport Processes, Vol. 41, Academic
916   Press, 1994.

917 [129] R. Gaur, L. Mishra, S. K. S. Gupta, Diffusion and transport of molecules in living cells, in: Modelling and
918   Simulation of Diffusive Processes, Springer, 2014, pp. 27–49.

919 [130] S. G. Schultz, S. Schultz, Basic principles of membrane transport, Vol. 2, CUP Archive, 1980.

920 [131] W. Stein, Transport and diffusion across cell membranes, Elsevier, 2012.

921 [132] T. R. Shannon, K. S. Ginsburg, D. M. Bers, Reverse mode of the sarcoplasmic reticulum calcium pump and
922   load-dependent cytosolic calcium decline in voltage-clamped cardiac ventricular myocytes, Biophysical journal
923   78 (1) (2000) 322–333.

924 [133] R. Garay, P. Garrahan, The interaction of sodium and potassium with the sodium pump in red cells, The Journal
925   of Physiology 231 (2) (1973) 297–325.

926 [134] E. Delpire, K. B. Gagnon, Kinetics of hyperosmotically stimulated Na-K-2Cl cotransporter in xenopus laevis
927   oocytes, American Journal of Physiology-Cell Physiology 301 (5) (2011) C1074–C1085.

[135] T. Hartmann, A. Verkman, Model of ion transport regulation in chloride-secreting airway epithelial cells. integrated description of electrical, chemical, and fluorescence measurements, Biophysical journal 58 (2) (1990) 391–401.

[136] C. Y. Cha, C. Oka, Y. E. Earm, S. Wakabayashi, A. Noma, A model of Na+/H+ exchanger and its central role in regulation of pH and Na+ in cardiac myocytes, Biophysical journal 97 (10) (2009) 2674–2683.

[137] A. M. Weinstein, A mathematical model of the outer medullary collecting duct of the rat, American Journal of Physiology-Renal Physiology 279 (1) (2000) F24–F45.

[138] Y. Sohma, M. Gray, Y. Imai, B. Argent, A mathematical model of the pancreatic ductal epithelium, The Journal of membrane biology 154 (1) (1996) 53–67.

[139] H. W. Florey, The transport of materials across the capillary wall, Quarterly Journal of Experimental Physiology and Cognate Medical Sciences: Translation and Integration 49 (2) (1964) 117–128.

[140] J. Aroesty, J. F. Gross, Convection and diffusion in the microcirculation, Microvascular research 2 (3) (1970) 247–267.

[141] C. Michel, Fluid exchange in the microcirculation, The Journal of physiology 557 (3) (2004) 701–702.

[142] Y. Himeno, M. Ikebuchi, A. Maeda, A. Noma, A. Amano, Mechanisms underlying the volume regulation of interstitial fluid by capillaries: a simulation study, Integrative medicine research 5 (1) (2016) 11–21.

[143] D. Zinemanas, R. Beyar, S. Sideman, Relating mechanics, blood flow and mass transport in the cardiac muscle, International journal of heat and mass transfer 37 (1994) 191–205.

Declaration of Competing Interest

There are no conflicts of interest to declare.

Funding

1